KfK 2699
Oktober 1978

Creep Rupture at Non-steady Stress and Temperature Loading Conditions

M. Boček
Institut für Material- und Festkörperforschung
Projekt Nukleare Sicherheit

Kernforschungszentrum Karlsruhe

KERNFORSCHUNGSZENTRUM KARLSRUHE GMBH
ISSN 0303-4003

KERNFORSCHUNGSZENTRUM KARLSRUHE

Institut für Material- und Festkörperforschung
Projekt Nukleare Sicherheit

KfK - 2699

Creep Rupture at Non-steady Stress- and Temperature Loading Conditions

von

M. Boček

Kernforschungszentrum Karlsruhe G.m.b.H., Karlsruhe

Abstract

Assuming the validity of the life fraction rule (LFR) the time to rupture as well as the respective stress and temperature at failure have been calculated for several ramp loading conditions. The results of ramp rupture tests can be predicted solely from iso-stress rupture experiments without any fitting procedure. The calculations are compared with results from tube burst experiments as well as with those from tensile tests on Zircaloy-4. For this material the LFR is obeyed in the temperature range examined (873K ÷ 1110K). The agreement between the calculations and the experimental results is surprisingly good. As compared to iso-rupture tests the reproducibility of the results of ramp-rupture tests is substantially improved. From a model of RAJ and ASHBY developed for ductile intercrystalline failure it can be shown that the LFR is obeyed as far as the appropriate damage function behaves as a function of state.

Das Zeitstandverhalten bei nicht stationären Spannungs- und Temperaturbelastungen

Unter der Anahme der Gültigkeit der Summenregel der Lebensanteile (SRL) wurde die Standzeit und die entsprechende Bruchspannung sowie Bruchtemperatur für verschiedene Rampen-Beanspruchungen berechnet. Die Ergebnisse solcher Versuche können allein an Hand von iso-Standzeitversuchen ohne jegliche Anpassungsverfahren vorhergesagt werden. Die Berechnungen werden mit experimentellen Ergebnissen verglichen, die sowohl an Zircaloy-4 Hüllrohren als auch an Zugproben gewonnen wurden. Für diesen Werkstoff ist die SRL im untersuchten Temperaturintervall (873K÷1110K) erfüllt. Die Übereinstimmung zwischen Rechnungen und Experiment ist überraschend gut. Die Reproduzierbarkeit der Ergebnisse aus Rampenversuchen ist wesentlich besser als die von iso-Standzeitversuchen. Dynamische Rekristallisation bewirkt Abweichungen von der SRL. Argumente für die den Rechnungen zugrundeliegenden Annahmen können dem Modell von RAJ und ASHBY entnommen werden. Es wird gezeigt, daß die SRL befolgt wird, wenn die entsprechende Schadensfunktion die Eigenschaft einer Zustandsfunktion aufweist.

CONTENTS

1. Introduction

2. Theoretical
2.1 Simple Ramps
2.1.1 The Temperature Ramp
2.1.1.1 The Equivalent Temperature at Failure $T_{B,eq.}$
2.1.1.2 The T_o-sensitivity of the Temperature at Failure $\tilde{T}_B$
2.1.1.3 The σ_o-sensitivity of $\tilde{T}_B$
2.1.1.4 The c-sensitivity of the Life Time $\tilde{\tau}_\sigma$
2.1.2 The Stress Ramp
2.1.2.1 The Equivalent Stress at Failure $\sigma_{B,eq.}$
2.1.2.2 The σ_o-sensitivity of the Stress at Failure $\tilde{\sigma}_B$
2.1.2.3 The b-sensitivity of $\tilde{\sigma}_B$ and the Correction of $\tilde{\sigma}_B$ for Constant Loading Rate b_o
2.1.2.4 The Connection Between $\sigma_{B,eq.}$ and $T_{B,eq.}$
2.2 Superimposed Ramps
2.3 Combined Ramps
2.3.1 The T-Ramp-Hold Procedure
2.3.2 The Double T-Ramp
2.3.3 The σ-Ramp-Hold Procedure
2.3.4 The Double σ-Ramp

3. Experimental
3.1 The Temperature Ramp
3.2 The Stress Ramp

4. Discussion
4.1 Model Considerations
4.2 Applications to Zircaloy
4.2.1 Failure Prediction
4.2.2 Comparison to Experiments
4.3 General Conclusions

5. Summary

1. Introduction

In designing structures which are to be subjected to varying loads and temperatures it is important to know what is the life time of materials crept under non-steady loading conditions.

This problem has been treated in the past especially with regard to cyclic stress and temperature variations. For a review of the elder literature as well as for a general formulation of the problem the reader is refered to the paper of TAIRA [1] .

The impetus to this investigation was given by the problem of the prediction of the inelastic behavior of fuel rods in light water reactors (LWR's) subjected to off- normal loading conditions. For information on this field the reader is refered to special publications e.g. [2] .

The actual problem with which this paper is concerned is to predict the life time of structures subjected to superimposed stress-temperature ramps. The calculations will be compared with results from tube burst experiments as well as with those from tensile tests on Zirkaloy-4.

2. Theoretical

2.1 Simple Ramps

2.1.1 The Temperature Ramp

The attempts to predict the life in creep rupture under varying temperatures (transient tests) from the data of creep rupture under constant temperature (iso-tests) are rather old. For this purpose ROBINSON [3] in the late thirtees first used the concept of the l i f e f r a c t i o n s . On the basis of this idea nowadays stress ramps and stress rupture at cycling temperature has been repeatedly treated (see e.g.[5]and [6]).

The so-called life fraction rule (LFR) will be shortly explained by the following example. For an experiment in which at constant load the temperature is step-wise increased $T_0 \rightarrow T_1 \rightarrow T_2 \rightarrow \ldots$ it is assumed that

$$\frac{\Delta t}{\tau_0}+\frac{\Delta t}{\tau_1}+\ldots+\frac{\Delta t}{\tau_B} = 1 \qquad (2.1.1a)$$

or

$$\Delta t \sum_{T_i=T_0}^{T_i=\tilde{T}_B} \left[\frac{1}{\tau_i}\right]_\sigma = 1 \qquad (2.1.1b)$$

Where τ_i is the iso-life time at the temperature T_i, Δt is the time the sample spent at T_i (assumed to be equal for all T_i). $\tilde{T}_B$ is the unknown temperature of failure which for a given stress depends on Δt.

The terms in Eq (2.1.1) are the life fractions which are considered as being mutually independent. As will be shown in chapter 4.1 the individual terms in Eq (2.1.1a) are considered as being representative for the material damage. In the probabilistic interpretation each term of Eq (2.1.1a) is the fractio-

nal probability for failure to occur in the i-th step at a stress σ_0 and temperature T_i in Δt seconds.
With increasing step number the total probability for fracture increases and equals one at fracture. This is the content of the life fraction rule.

Rewriting Eq (2.1.1b) in the infinitesimal form, it is

$$\int_{T_0}^{\tilde{T}_B} \frac{dt}{\tau[T(t)]} = 1 \; . \qquad (2.1.2)$$

As mentioned above the LFR can be substantiated by micro-models (see chapter 4.1), however its validity for a particular case has to be checked experimentally.

To solve Eq (2.1.2) for $\tilde{T}_B$ we substitute for

$$dt = \frac{dT}{c} \qquad (2.1.3)$$

and insert for $\tau(T)_\sigma$ the results from iso-creep tests which generally are of the form (see e.g. [4])

$$\frac{T}{T-T_0} \ln {}^{\tau_0}/_{\tau} = P(T_0) = \frac{Q}{RT_0} > 0 \qquad (2.1.4)$$

For Zircaloy-4 this relation is derived from Fig.1. $\tau<\tau_0$ are the life times at the temperatures $T>T_0$ respectively; P is the Larson-Miller parameter depending on T_0; Q is the apparent activation energy for the high temperature creep; R has the usual meaning.

Assuming the heating rate c=const.$\neq$f(T) we obtain

$$\int_{T_0}^{\tilde{T}_B} e^{P(1-T_0/T)} \, dT = \tau_0 c \qquad (2.1.5)$$

The integral in this form divergates. Using the modified function, however

$$\frac{T}{T-T_0} \ln \tau_0/\tau^* = -\ln\left[\frac{KT}{PT_0} + 1\right] = P \qquad \text{for } T_0 \neq T \tag{2.1.6}$$

the solution of the integral in Eq (2.1.5) remains finite for K=2. Comparing both the functions Eq (2.1.4) and Eq (2.1.6), it is because $\frac{KT}{PT_0} << 1$ (for Zircaloy see chapter 4.2).

$$\tau^*(T) \equiv \tau(T). \tag{2.1.7}$$

Inserting Eq (2.1.6) instead of Eq (2.1.4) into Eq (2.1.5) we obtain for

$$c = \text{const.} \neq f(T) \tag{2.1.8}$$

$$\frac{Pc\tau_0}{T_0} + 1 = \left[\left(\frac{\tilde{T}_B}{T_0}\right)^2 e^{P(1-T_0/\tilde{T}_B)}\right]_{\sigma_0, c} \qquad \text{for } T_0 \neq \tilde{T}_B \tag{2.1.9}$$

The ramp-life time $\tilde{\tau}_\sigma$ follows then from

$$\tilde{\tau}_\sigma = \frac{\tilde{T}_B - T_0}{c}. \tag{2.1.10}$$

$\tilde{T}_B$ or $\tilde{\tau}_\sigma$ are calculated as functions of c only by the use of iso-test data.

From the functions $\tilde{T}_B(c)_{\sigma_0}$ (Fig.4) and $\tilde{\tau}(c)_{\sigma_0}$ (Fig.3) the functions $\tilde{T}_B(\sigma_0)_c$ and $\tilde{\tau}(\sigma_0)_c$ are obtained. These are shown in Fig.2 and Fig.5 respectively.

Because the initial values of the ramp $\dot{\tau}_0$ and T_0 determine the stress σ_0 (see Fig.1) in the temperature ramp test, it follows from Eq(8) that $\tilde{T}_B$ or $\tilde{\tau}_\sigma$ respectively are functions of σ_0 too.

In praxis the T-ramps are seldom linear. For this case the solution given by Eq (2.1.9) can be used only as an approximation. However, Eq (2.1.2) can be integrated analytically also for e.g.

$$c=\gamma T. \tag{2.1.11}$$

Using Eq (2.1.6) with K=1 one obtains inserting Eq (2.1.6) together with $dt=\frac{dT}{\gamma T}$ into Eq (2.1.2)

$$P\gamma\tau_0 + 1 = \left[\frac{\tilde{T}_B}{T_0}\, e^{P(1-T_0/\tilde{T}_B)}\right]_{\sigma_0,\gamma} \quad ; \; T_0 \neq \tilde{T}_B \tag{2.1.12}$$

It can be realized comparing Eq (2.1.9) with Eq (2.1.12) that even for very small γ-values the non-linearity of the T-ramp influences the $\tilde{T}_B$-values very sensitively.

2.1.1.1 The Equivalent Temperature at Failure $T_{B,Eq}$.

An equivalent temperature at failure $T_{B,eq}$ can be introduced by the relations

$$T_{B,eq}\Big|_{\sigma_0} = \tilde{T}_B\Big|_{\sigma_0} \tag{2.1.13a}$$

and

$$\tau\Big|_{T_{B,eq},\sigma_0} = \tilde{\tau}\Big|_{\tilde{T}_B,\sigma_0} \tag{2.1.13b}$$

Thus $T_{B,eq}$ is defined as the temperature in the iso-stress rupture test which at the same stress σ_0 leads to the same life time τ as the observed one in the temperature ramp test $\tilde{\tau}_\sigma$.

From Eq (2.1.9)

$$P=(1-T_0/\tilde{T}_B)=\ln\left[\frac{Pc\tau_0}{T_0} + 1\right] - 2\ln \tilde{T}_B/T_0$$

together with Eqs.(2.1.4) and (2.1.13b)

$$P\left(1-T_0/T_{B,eq}\right)= \ln^{\tau 0}/_{\tau} = \ln^{\tau 0}/_{\tilde{\tau}}$$

it follows due to Eq (2.1.13a) that

$$2\ln \frac{T_{B,eq}}{T_0} = \ln\left(\frac{Pc\tau_0}{T_0} + 1\right) - \ln^{\tau 0}/_{\tau}$$

and therefrom we obtain

$$T_{B,eq} = T_0\sqrt{\frac{\tau}{\tau_0}\left(\frac{Pc\tau_0}{T_0} + 1\right)}, \text{ for } T_0 \neq T_{B,eq}. \qquad (2.1.14)$$

As far as $c >> \frac{T_0}{P\tau_0}$, it is

$$T_{B,eq} \doteq \sqrt{T_0 Pc\tau} \qquad (2.1.15)$$

Thus choosing $\tau=\tilde{\tau}$ the value for the temperature at failure $\tilde{T}_B=T_{B,eq}$ for this life time can be calculated using iso-test data only.

2.1.1.2 The T_0-sensitivity of the Temperature at Failure $\tilde{T}_B$.

It follows from Eq (2.1.9) that

$$d\tilde{T}_B \doteq \frac{1 - \frac{2}{P}}{1 + \frac{1}{P}\ln\frac{T_0}{Pc\tau_0}} dT_0 \qquad (2.1.16)$$

which to a good approximation gives

$$d\tilde{T}_B \doteq dT_0 \qquad (2.1.17)$$

independent upon heating rate.

The change of $\tilde{\tau}_\sigma$ due to a change in $\tilde{T}_B$ is according to Eq (2.1.10)

$$d\tilde{\tau}_\sigma = \frac{d\tilde{T}_B}{c} \qquad (2.1.18)$$

From Eq (2.1.17) we obtain

$$d\tilde{\tau}_\sigma \doteq \frac{1}{c}\, dT_0 \qquad (2.1.19)$$

Thus the influence of an change in T_0 upon $\tilde{\tau}_\sigma$ decreases with increasing heating rate.

2.1.1.3 The σ_0-Sensitivity of $\tilde{T}_B$

According to Eq (2.1.9) $\tilde{T}_B$ is not explicitly dependent upon σ_0. However σ_0 enters the Eq (2.1.9) through τ_0 and T_0. For T_0=constant it follows from iso-stress rupture experiments [4]

$$n \ln\left(\frac{\sigma_0}{\sigma_0^*}\right)_{T_0} = \ln\left(\frac{\tau_0^*}{\tau_0}\right)_{T_0} \qquad (2.1.20)$$

Where σ_0^*, τ_0^* are considered as fixed values and $^1/_n$ is the slope in the stress rupture diagram.

Therefrom it follows that

$$\left(\frac{d\tau_0}{\tau_0}\right)_{T_0} = -n\left(\frac{d\sigma_0}{\sigma_0}\right)_{T_0} \qquad (2.1.21)$$

where τ_0, σ_0 stays instead of τ_0^* and σ_0^* respectively.

From Eq (2.1.9) we obtain

$$\left(\frac{d\tau_0}{\tau_0}\right)_{T_0} = \frac{1}{c\tau_0}\left[\frac{2}{P}\left(\frac{\tilde{T}_B}{T_0}\right)^2 e^{P(1-T_0/\tilde{T}_B)} + 1\right]_{T_0} d\tilde{T}_B \quad . \qquad (2.1.22)$$

Inserting Eq (2.1.21) it is

$$-\frac{d\sigma_0}{\sigma_0} = \frac{1}{cn\tau_0}\, e^{P(1-T_0/\tilde{T}_B)} \left[\frac{2}{P}\,\frac{\tilde{T}_B}{T_0} + 1\right] d\tilde{T}_B \qquad (2.1.23a)$$

or

$$-\frac{d\sigma_0}{\sigma_0} \doteq \frac{1}{cn\tau_0}\, e^{P(1-T_0/\tilde{T}_B)} \cdot d\tilde{T}_B \qquad (2.1.23b)$$

respectively.

Inserting for $\tilde{T}_B$ and $d\tilde{T}_B$ from Eq (2.1.10) into Eq (2.1.23b) one obtains

$$-\frac{d\sigma_0}{\sigma_0} \doteq \frac{1}{n\tau_0}\, e^{P\left[1-\frac{T_0}{T_0+c\tilde{\tau}}\right]} \cdot d\tilde{\tau} \qquad (2.1.23c)$$

As will be shown later in chapter 4.2.2 experimental $(\sigma_0-\tilde{\tau}_\sigma)$-diagrams can be analysed by means of Eq (2.1.23c).

Several consequences follow from Eqs.(2.1.23):

1. For a deviation $d\tilde{T}_B$ from the calculated temperature $\tilde{T}_B$ it is

   $d\sigma_0<0$ for $d\tilde{T}_B>0$ (2.1.24a)

   and

   $d\sigma_0>0$ for $d\tilde{T}_B<0$ (2.1.24b)

2. For a given value of $d\tilde{T}_B$

   - $d\sigma_0 \sim \sigma_0$
   - $d\sigma_0$ increases with increasing $\tilde{T}_B$
   - $d\sigma_0$ decreases with increasing c.

Eqs. (2.1.23) are of considerable practical importance. In T-ramp experiments the determination of the true burst temperature $\tilde{T}_B$ is a difficult problem depending on the heating modus as well as on the temperature measurement itself. Thus Eq(2.1.23b) may be a useful tool for comparing experimental results from T-ramp tests with calculations (see chapter 3.1).

2.1.1.4 The c-Sensitivity of $\tilde{T}_B$ and $\tilde{\tau}_\sigma$.

For $\tilde{T}_B << \frac{PT_0}{2}$ it follows from Eq(2.1.9)

$$d\tilde{T}_B \doteq \tau_0 e^{-P(1-T_0/\tilde{T}_B)} \cdot dc \qquad (2.1.25)$$

Thus $d\tilde{T}_B$ is independent upon c, but for given dc, $d\tilde{T}_B$ decreases as $\tilde{T}_B$ increases. Inserting for $\tilde{T}_B$ from Eq(2.1.10) into Eq(2.1.9) we obtain

$$\left(\frac{d\tilde{\tau}}{\tilde{\tau}}\right)_\sigma \doteq \frac{PT_0\tau_0}{c\tilde{\tau}_\sigma^2} e^{P\left[\frac{T_0}{T_0+c\tilde{\tau}_\sigma} - 1\right]} \cdot \frac{dc}{c} . \qquad (2.1.26)$$

From Eq(2.1.26) it follows that for a given $\frac{dc}{c}$

for $\tilde{\tau}_\sigma$=const. $\left.\frac{d\tilde{\tau}}{\tilde{\tau}}\right|_\sigma$ rapidly decreases as c increases

and

for c=const. $\left.\frac{d\tilde{\tau}}{\tilde{\tau}}\right|_\sigma$ decreases rapidly with increasing $\tilde{\tau}_\sigma$.

2.1.2 The Stress Ramp

In analogy to the temperature ramp test as far as the LFR is obeyed it should hold for a stress ramp test at constant temperature that

$$\int_{\sigma_0}^{\tilde{\sigma}_B} \frac{dt}{\tau[\sigma(t)]_T} = 1 \qquad (2.1.27)$$

where σ_0, $\tilde{\sigma}_B$ are the initial stress and the stress at failure respectively. Inserting for $\tau(\sigma)_T$ the result of iso-stress rupture tests [4]

$$\tau(\sigma) = \tau_0 \left(\frac{\sigma_0}{\sigma}\right)^n_{T=\text{const.}} \quad , \tag{2.1.28}$$

substituting for dt

$$dt = \frac{d\sigma}{b} \quad , \tag{2.1.29}$$

and inserting Eq(2.1.28) into Eq(2.1.27) we obtain for

$$b = \text{const.} \neq f(\sigma) \tag{2.1.30}$$

$$\tilde{\sigma}_B = \left\{ \sigma_0^{\,n} \left[b\tau_0 (n+1) + \sigma_0 \right] \right\}^{1/(n+1)}_{T_0, b} \quad . \tag{2.1.31}$$

In the case that

$$b >> \frac{\sigma_0}{\tau_0 (n+1)} \tag{2.1.32}$$

it is in dimensionless form

$$\left(\frac{\tilde{\sigma}_B}{\sigma_0}\right)^{n+1}_{T,b} \doteq \frac{b\tau_0 (n+1)}{\sigma_0} \quad . \tag{2.1.33}$$

Recalculating to the life time $\tilde{\tau}_T$

$$\tilde{\tau}_T = \frac{\tilde{\sigma}_B - \sigma_0}{b} \tag{2.1.34}$$

we obtain from Eq(2.1.27)

$$\tilde{\tau}_{T,B} = \left(\frac{\sigma_0}{b}\right)^{\frac{n}{n+1}} \left[\tau_0 (n+1)\right]^{1/(n+1)} - \frac{\sigma_0}{b} \quad . \tag{2.1.35}$$

The second term on the right hand side of Eq(2.1.35) can be neglected against the first one, thus in dimensionless form it is

$$\log\left(\frac{\tilde{\tau}}{\tau_0}\right)_{T,b} \doteq \frac{n}{n+1}\log\frac{\sigma_0}{b\tau_0} + \frac{1}{n+1}\log(n+1) \quad . \tag{2.1.36}$$

The dependence of $\tilde{\sigma}_B/\sigma_0$ upon the stress rate b is shown in Fig.6.

In contrast to $\tilde{T}_B$ for non-linear T-ramps the $\tilde{\sigma}_B$-values for non-linear σ-ramps are easily obtained analytically from the Eqs.(2.1.27) and (2.1.28). For e.g.

$$b(\sigma) = \beta\sigma \tag{2.1.37}$$

it follows for β=const. together with $dt = \frac{d\sigma}{\beta\sigma}$

$$\tilde{\sigma}_B = \sigma_0\left[(n+1)\beta\tau_0+1\right]^{1/n}_{T_0,\beta} \tag{2.1.38}$$

An analysis of the corresponding equations shows, that contrary to $\tilde{T}_B$-values, $\tilde{\sigma}_B$ is less influenced by the non-linearity of the ramp.

2.1.2.1 The Equivalent Stress at Failure $\sigma_{B,eq}$.

$\sigma_{B,eq}$ is defined as the stress in the iso-stress rupture test which at the same temperature T_0 leads to the same life time τ as the observed one in the stress ramp test $\tilde{\tau}_T$. This is expressed by the conditions

$$\sigma_{B,eq}\Big|_{\sigma_0} = \tilde{\sigma}_B\Big|_{\sigma_0} \tag{2.1.39a}$$

and

$$\tau\Big|_{\sigma_{B,eq},T_0} = \tilde{\tau}\Big|_{\tilde{\sigma}_B,T_0} \tag{2.1.39b}$$

According to Eq(2.1.28) it is

$$\log\tau/\tau_0 = -n\,\log\frac{\sigma_{B,eq}}{\sigma_0} \quad ; \tag{2.1.40}$$

combining Eqs.(2.1.40) and (2.1.36) it is due to Eq(2.1.39b)

$$\sigma_{B,eq} = \sigma_0 \left(\frac{\sigma_0}{b\tau_0}\right)^{-\frac{1}{n+1}} \cdot (n+1)^{-\frac{1}{n(n+1)}} \qquad (2.1.41)$$

Also $\sigma_{B,eq}$ can be calculated from the results of iso-stress rupture tests. The dependence of $\frac{\sigma_{B,eq}}{\sigma_0}$ upon $\frac{\sigma_0}{b\tau_0}$ is shown in Fig.8.

2.1.2.2 The σ_0-Sensitivity of the Stress at Failure $\tilde{\sigma}_B$.

From Eq(2.1.33) follows for b=const.

$$\left.\frac{d\tilde{\sigma}_B}{\tilde{\sigma}_B}\right|_T = \frac{n}{n+1} \left.\frac{d\sigma_0}{\sigma_0}\right|_T \qquad (2.1.42a)$$

or

$$d\tilde{\sigma}_B = \frac{n}{n+1} \frac{\tilde{\sigma}_B}{\sigma_0} d\sigma_0 \qquad (2.1.42b)$$

For the life time change it follows from Eq(2.1.34) and Eq(2.1.42b)

$$d\tilde{\tau}_T = \frac{d\tilde{\sigma}_B}{b} = \frac{n}{n+1} \frac{\tilde{\sigma}_B}{b} \frac{d\sigma_0}{\sigma_0} \qquad (2.1.43)$$

According to Eq(2.1.42a) the relativ change of $\tilde{\sigma}_B$ is practically independent upon n and is proportional to $\frac{d\sigma_0}{\sigma_0}$.
The change in life time caused by a change in σ_0 is, for a given relative change in σ_0 directly proportional to $\tilde{\sigma}_B$ and indirectly proportional to b.

2.1.2.3. The b-Sensitivity of $\tilde{\sigma}_B$ and the Correction of $\tilde{\sigma}_B$ for Constant Loading Rate b_0.

From Eq(2.1.33) it follows

$$\left.\frac{d\tilde{\sigma}_B}{\tilde{\sigma}_B}\right|_T = b^{\frac{1}{n+1}} \cdot \frac{(n+1)}{\tilde{\sigma}_B} \cdot (\sigma_0^n \tau_0) \cdot \frac{db}{b} \qquad (2.1.44)$$

Recalculation to $d\tilde{\tau}_T$ gives

$$\left.\frac{d\tilde{\tau}}{\tilde{\tau}}\right|_T = b^{-\frac{n}{n+1}} \cdot \frac{(n+1)}{\tilde{\tau}} \cdot (\sigma_0 \tau_0)^{\frac{1}{n+1}} \cdot \frac{db}{b} \qquad (2.1.45)$$

An analysis of Eqs.(2.1.44) and (2.1.45) leads to the following conclusions:

at given $\frac{d\sigma_0}{\sigma_0}$

$\left.\frac{d\tilde{\sigma}_B}{\tilde{\sigma}_B}\right|_T$ slightly increases with increasing b

and

$\left.\frac{d\tilde{\tau}}{\tilde{\tau}}\right|_T$ decreases very rapidly with increasing b.

Due to the change of sample geometry during plastic flow normally in a stress ramp experiment a c o n s t a n t l o a d r a t e is maintained

$$\dot{F} = S_0 b_0 \qquad (2.1.46a)$$

where S_0 is the crossectional area of the sample and b_0 the stress rate at the start of the ramp. Because S is a function of the plastic strain e for a constant stress ramp, Eq(2.1.46a) modifies to

$$\dot{F} = S(e) b_0 \qquad (2.1.46b)$$

Assuming u n i f o r m s t r a i n and the p r e s e r -

v a t i o n o f v o l u m e it is

$$S(e) = S_0 (1+e) \tag{2.1.47}$$

Inserting this into Eq(2.1.46b) and comparing with Eq(2.1.46a) we have

$$\frac{\dot{F}}{S_0} = b_0(1+e) = b \tag{2.1.48}$$

Eq(2.1.48) into Eq(2.1.33) gives

$$\tilde{\sigma}_B^{n+1} = \sigma_0^{\,n} \tau_0 (n+1) b_0 (1+e_B) \tag{2.1.49}$$

where e_B is the nominal plastic strain at failure. Because the true strain ε is definded as

$$\varepsilon = \ln(1+e) \ , \tag{2.1.50}$$

the combination of Eqs(2.1.50) and (2.1.49) yields for ε_B in a stress ramp test at constant temperature

$$\varepsilon_B = (n+1) \ln \frac{\tilde{\sigma}_B}{\sigma_0} - \ln \frac{b_0 \tau_0}{\sigma_0} - \ln(n+1) \tag{2.1.51}$$

A comparison with experimental results on σ-tensile ramped Zircaloy-4 [11] has shown, that the calculated ε_B-values are as six times as large as the experimental ones. This discrepancy is explained by the abundant necking of the failed specimens in the way that Eq(2.1.47) is not obeyed for strains larger than the uniform strain.

2.1.2.4 The Connection Between $\sigma_{B,eq}$ and $T_{B,eq}$.

Considering a σ-ramp for which the life times

$$\tilde{\tau}_T = \tilde{\tau}_\sigma = \tilde{\tau} \tag{2.1.52}$$

where $\tilde{\tau}_\sigma$ is the life time of the "corresponding" T-ramp. It follows from the Eqs.(2.1.4) and (2.1.28) for the equivalent stress and temperature

$$n \ln \frac{\sigma_{B,eq}}{\sigma_0} = P(1-T_0/T_{B,eq}) \qquad (2.1.53)$$

inserting from the Eqs.(2.1.41) and (2.1.13) respectively and recalling the definition equation

$$\tilde{t} = \tau \qquad (2.1.39b)$$

it is

$$n \ln \frac{\sigma_0}{b\tau_0} = -(n+1)\left[\frac{P}{n}\left(1-\sqrt{\frac{T_0}{Pc\tau}}\right) + \frac{1}{n(n+1)} \ln(n+1)\right] \qquad (2.1.54)$$

what approximately yields

$$\sigma_0 \doteq b\tau_0 e^{-\frac{n+1}{n^2} P\left\{1-\sqrt{T_0/Pc\tau}\right\}} \qquad (2.1.55a)$$

or

$$T_0 \doteq Pc\tau \left\{1 + \frac{n^2}{n+1} \frac{1}{P} \ln \frac{\sigma_0}{b\tau_0}\right\}^2 \qquad (2.1.55b)$$

The Eqs(2.1.55) describe the condition of an iso-stress rupture test with the same life time as that corresponding to a pair of σ- and T-ramp tests for which Eq(2.1.52) is obeyed. The iso-stress σ_0 is connected to the corresponding T_0-value by the ramp test conditions(b,c,n,P,τ_0). Because σ_0 is determined by T_0 and τ_0 (see Fig.1) and P is determined by T_0, there is only one pair of σ_0-, T_0-values for one pair of σ- and T-ramp tests which satisfy the condition of Eq(2.1.52).

2.2 Superimposed Ramps.

To treat this problem again the validity of the life fraction rule is assumed. We further suppose that the ramps can be superimposed independently. For a ductile failure machanism there are theoretical arguments (see chapter 4.1) which support this assumption.

The basic equation is now

$$\frac{1}{c}\int_{T_0}^{s\tilde{T}_B}\frac{dT}{\tau[T(t)]_\sigma}+\frac{1}{b}\int_{\sigma_0}^{s\tilde{\sigma}_B}\frac{d\sigma}{\tau[\sigma(t)]_T}=1 \qquad (2.2.1)$$

The unknown is ${}^s\tilde{T}_B$ or ${}^s\tilde{\sigma}_B$ respectively. Knowing one, the other is determined from (see Fig.8)

$${}^s\tilde{\sigma}_B=\sigma_0+\frac{b}{c}\left({}^s\tilde{T}_B-T_0\right) \qquad (2.2.2a)$$

$${}^s\tilde{T}_B=T_0+\frac{c}{b}\left({}^s\tilde{\sigma}_B-\sigma_0\right) \qquad (2.2.2b)$$

The solutions of the integrals in Eq(2.2.1) are given by Eqs. (2.1.9) and (2.1.31) respectively. Substituting for ${}^s\tilde{\sigma}_B$ (Eq.2.2.2a) we obtain

$$\frac{c}{b}\frac{P}{T_0\sigma_0^{\,n}(n+1)}\left\{\sigma_0+\frac{b}{c}\left\{{}^s\tilde{T}_B-T_0\right\}\right\}^{n+1}+\left[\frac{{}^s\tilde{T}_B}{T_0}\right]^2 e^{P\left(1-T_0/{}^s\tilde{T}_B\right)}= \qquad (2.2.3)$$

$$=1+\frac{P\tau_0 c}{T_0}+\frac{c}{b}\frac{P\sigma_0}{T_0(n+1)}$$

Therefrom ${}^{s}\tilde{T}_B$ is obtained by computing the ratio c/b as a function of ${}^{s}\tilde{T}_B$ for fixed c-values and for given T_0, P, $n(T_0)$, P,σ_0 (see Fig.9). Eq(2.2.3) reduces for

$$\frac{\sigma_0}{{}^{s}\tilde{T}_B - T_0} >> \frac{b}{c} \tag{2.2.4}$$

to

$$\frac{P\tau_0 c}{T_0} + 1 = \left(\frac{{}^{s}\tilde{T}_B}{T_0}\right)^2 e^{P(1-T_0/{}^{s}\tilde{T}_B)} \quad , \quad T_0 \neq {}^{s}\tilde{T}_B \tag{2.2.5}$$

which is identical with Eq(2.1.9) for

$${}^{s}\tilde{T}_B = \tilde{T}_B \quad . \tag{2.2.6}$$

Thus the condition given by Eq(2.2.4) specifies by means of the ratio $\frac{b}{c}$ two cases.

In the first case when Eq(2.2.4) is satisfied, the influence of the stress ramp on ${}^{s}\tilde{T}_B$ and thus on life time ${}^{s}\tilde{\tau}$ can be neglected, the T-ramp is dominating.

In the second case ${}^{s}\tilde{T}_B$ is determined by both contributions. We approximate the brackett term in Eq(2.2.3)

$$\left[1+\frac{b}{c}\,\frac{{}^{s}\tilde{T}_B - T_0}{\sigma_0}\right]^{n+1} = 1+\frac{b}{c}\,\frac{{}^{s}\tilde{T}_B - T_0}{\sigma_0} + \frac{1}{2}\left[\frac{b}{c}\,\frac{{}^{s}\tilde{T}_B - T_0}{\sigma_0}\right]^2 + \ldots \tag{2.2.7}$$

Inserting Eq(2.2.7) into Eq(2.2.3) and for $\frac{P\tau_0 c}{T_0} >> 1$ it is finally

$$\frac{c}{b} = \frac{\frac{P\sigma_0}{T_0(n+1)}\left[\frac{{}^{s}\tilde{T}_B - T_0}{\sigma_0}\right]^2}{2\left[\frac{P\tau_0 c}{T_0} - \frac{P}{T_0}\,\frac{{}^{s}\tilde{T}_B - T_0}{(n+1)} - \left(\frac{{}^{s}\tilde{T}_B}{T_0}\right)^2 e^{P(1-T_0/{}^{s}\tilde{T}_B)}\right]} \tag{2.2.8}$$

In Fig.9 the results are shown for the case of relatively high b-values.

2.3 Ramp-Hold Procedures

The material loading procedures schematically shown in Figures 10 and 11 respectively, could be practically important e.g. in the heat-up phase of a LOCA. The aim of the present task is to calculate the total life times $\tilde{\tau}^{*}_{\sigma,T}$ of ramp hold tests.

2.3.1 The T-Ramp-Hold Procedure

For a T-ramp-hold loading schema shown in Fig.11 the condition following from the LFR is

$$\int_{t_0}^{\tilde{t}_{1,\sigma}} \frac{dt}{\tau[T(t)]_\sigma} + \frac{t^{*}_{1,\sigma}}{\tau_{1,\sigma}} = 1 \qquad (2.3.1a)$$

where the meaning of the symbols is explained in Fig.11. Substituting for dt Eq(2.1.3) into Eq(2.3.1a) we obtain

$$\int_{T_0}^{T_1} \frac{dT}{\tau(T)_\sigma} = c\left[1 - \frac{t^{*}_{1,\sigma}}{\tau_{1,\sigma}}\right] . \qquad (2.3.1b)$$

It is further

$$\int_{T_0}^{T_1} \frac{dT}{\tau(T)_\sigma} = c - \int_{T_1}^{\tilde{T}_B} \frac{dT}{\tau(T)_\sigma} \qquad (2.3.2)$$

The solution of the integral on the right hand side of Eq(2.3.2) is given by Eq(2.1.9). The combination of Eqs.(2.1.9)(2.3.2) and (2.3.1b) leads to

$$t^{*}_{1,\sigma} = \frac{T_1}{P(T_1)c}\left[\left(\frac{\tilde{T}_B}{T_1}\right)^2 e^{P(T_1)(1-T_1/\tilde{T}_B)} - 1\right]_{\sigma,c} , \qquad (2.3.3)$$

where $t^{*}_{1,\sigma}$ turns out to be independent upon τ_1. According to Fig.11 it is

$$\tilde{\tau}^{*}_{\sigma} = \tilde{t}_{1,\sigma} + t^{*}_{1,\sigma} = \frac{T_1 - T_0}{c} + t^{*}_{1,\sigma} \qquad (2.3.4)$$

inserting Eq(2.3.3) into Eq(2.3.4) we obtain finally

$$\tilde{\tau}^{*}_{\sigma} = \frac{T_1}{c}\left\{1 - \frac{T_0}{T_1} + \frac{1}{P(T_1)}\left[\left(\frac{\tilde{T}_B}{T_0}\right)^2 e^{P(T_1)(1-T_0/\tilde{T}_B)} - 1\right]\right\}_{\sigma,c} \qquad (2.3.5)$$

For life time predictions in the case of a ramp-hold-test we need as compared to a simple ramp test in addition the holding temperature T_1 and instead of the $P(T_0)$ the value $P(T_1)$.

2.3.2 The Double T-Ramp

On the basis of the LFR it holds for T-Ramps shown in Fig.12

$$\frac{1}{c_1}\int_{T_0}^{T_1} \frac{dT}{\tau(T)_\sigma} + \frac{1}{c_2}\int_{T_1}^{{}^{D}\tilde{T}_B} \frac{dT}{\tau(T)_\sigma} = 1 \qquad (2.3.6)$$

where ${}^{D}\tilde{T}_B$ is the life time of the material subjected to the double T-ramp and T_1 the temperature at which c is changed. It holds further for ${}^{D}\tilde{T}_B \neq T_1$ (see Eq(2.1.9))

$$\frac{1}{c_1}\int_{T_0}^{T_1} \frac{dT}{\tau(T)_\sigma} = 1 - \frac{1}{c_1}\int_{T_1}^{\tilde{T}_B} \frac{dT}{\tau(T)_\sigma} =$$

$$= 1 - \frac{T_1}{P(T_1)\tau_1 c_1}\left[\left(\frac{\tilde{T}_B}{T_1}\right)^2 e^{P(T_1)\left\{1 - T_1/\tilde{T}_B\right\}} - 1\right]_{\sigma,c_1}. \qquad (2.3.7)$$

The solution (for $T_1 \neq {}^{D}\tilde{T}_B$) follows from inserting Eq(2.3.7) into Eq(2.3.6) together with

$$\frac{1}{c_2}\int_{T_1}^{D\tilde{T}_B}\frac{dT}{\tau(T)\sigma} = \frac{T_1}{P(T_1)\tau_1 c_2}\left[\left(\frac{D\tilde{T}_B}{T_1}\right)^2 e^{P(T_1)[1-T_1/D\tilde{T}_B]} - 1\right]_{\sigma,c_2} \qquad (2.3.8)$$

Two cases can be considered:

- $D\tilde{T}_B \gtrsim T_1$ (2.3.9a)

and

- $D\tilde{T}_B >> T_1$ (2.3.9b)

For the first case the solution is

$$\left(\frac{D\tilde{T}_B}{T_1}\right)^2 e^{P(T_1)[1-T_1/D\tilde{T}_B]} = \frac{c_2}{c_1} E(T_1, \tilde{T}_B) + 1 \qquad (2.3.10)$$

where

$$E = \left(\frac{\tilde{T}_B}{T_1}\right)^2 e^{P(T_1)[1-T_1/\tilde{T}_B]} .$$

From Eq(2.3.10) $D\tilde{T}_B$ follows as

$$F(D\tilde{T}_B)_{T_1,\tilde{T}_B} = \frac{c_1}{c_2} \quad (\text{for } D\tilde{T} \gtrsim T_1) \qquad (2.3.11)$$

In this case for a given ratio $\frac{c_1}{c_2}$ and a fixed $\tilde{T}_B$-value (for the simple T-ramp test)

$$D\tilde{T}_B = f(T_1)_{\tilde{T}_B, c_1/c_2} . \qquad (2.3.12)$$

For the case that

- $D\tilde{T}_B >> T_1$ (2.3.13)

it results recalling Eq(2.1.4)

$$\frac{c_1}{c_2} = \left(\frac{D\tilde{T}_B}{\tilde{T}_B}\right)^2 e^{Q/R\,\frac{\tilde{T}_B - D\tilde{T}_B}{D\tilde{T}_B\ \tilde{T}_B}} \qquad \text{for } D\tilde{T}_B >> T_1 \qquad (2.3.14)$$

Thus in this case

$$^{D}\tilde{T}_B \neq f(T_1) \tag{2.3.15}$$

the life time $^{D}\tilde{\tau}_\sigma$ for the double T-ramp follows from the equations

$$^{D}\tilde{\tau}_\sigma = t_1 + \frac{^{D}\tilde{T}_B - T_1}{c_2} \tag{2.3.16a}$$

and

$$t_1 = \frac{T_1 - T_0}{c_1} \tag{2.3.16b}$$

therefrom

$$^{D}\tilde{\tau}_\sigma = \frac{^{D}\tilde{T}_B}{c_2} + T_1\left(\frac{1}{c_1} - \frac{1}{c_2}\right) - \frac{T_0}{c_1} \quad . \tag{2.3.17}$$

An analysis of Eq(2.3.17) shows that

$$\text{for} \quad \tilde{T}_B > {}^{D}\tilde{T}_B$$

$$\text{is} \quad \frac{c_1}{c_2} > 1$$

and therefore

$$^{D}\tilde{\tau}_\sigma - \tilde{\tau}_\sigma \equiv \Delta\tilde{\tau}_\sigma > 0 \tag{2.3.18}$$

$$\text{for} \quad \tilde{T}_B < {}^{D}\tilde{T}_B$$

$$\text{is} \quad \frac{c_1}{c_2} < 1$$

and therefore

$$\Delta\tilde{\tau}_\sigma < 0 \; . \tag{2.3.19}$$

Analogical results hold for the double σ-ramp when $\tilde{\tau}_\sigma$-values are replaced by the corresponding $\tilde{\tau}_T$-values and c is replaced by b (see chapter 2.3.4).

2.3.3 The σ-Ramp-Hold-Procedure

In analogy to the procedure above in combination with Eq(2.1.31) we obtain

$$t^{*}_{1,T} = \left(\frac{\tilde{\sigma}_B}{\sigma_1}\right)^{n+1} \frac{\sigma_1}{b(n+1)} \left[1 - \left(\frac{\sigma_1}{\tilde{\sigma}_B}\right)^{n+1} \right]_T , \qquad (2.3.20)$$

which again is independent upon τ_1. The total life time is given by

$$\tilde{\tau}^{*}_{T} = \frac{\sigma_1}{b} \left\{ 1 - \frac{\sigma_0}{\sigma_1} + \frac{1}{n+1} \left[\left(\frac{\tilde{\sigma}_B}{\sigma_1}\right)^{n+1} - 1 \right] \right\}_T \qquad (2.3.21)$$

2.3.4 The Double σ-Ramp.

The problem is treated in the same way as for the double T-ramp. Again two cases are to be considered

a) $D\tilde{\sigma}_B \gtrsim \sigma_1$ (2.3.22a)

b) $D\tilde{\sigma}_B >> \sigma_1$ (2.3.22b)

The general solution is

$$\left(\frac{\tilde{\sigma}_B}{D\tilde{\sigma}_B}\right)^{n+1} = \frac{b_1}{b_2} \frac{1 - \left(\frac{\sigma_1}{\tilde{\sigma}_B}\right)^{n+1}}{1 - \left(\frac{\sigma_1}{D\tilde{\sigma}_B}\right)^{n+1}} \qquad (2.3.23)$$

For the case a) it is for $\tilde{\sigma}_B >> \sigma_1$

$$\left[D\tilde{\sigma}_B - \frac{\sigma_1}{n+1} \left(\frac{\sigma_1}{D\tilde{\sigma}_B}\right)^{n} \right]_{T,b_1,b_2} \doteq \tilde{\sigma}_B \left(\frac{b_2}{b_1}\right)^{\frac{1}{n+1}} \qquad (2.3.24)$$

where ${}^{D}\tilde{\sigma}_B$ is the stress at failure for the double σ-ramp and σ_1 is the stress at which the rate b has been changed.
Thus for this case

$$ {}^{D}\tilde{\sigma}_B = f(\sigma_1)\,\tilde{\sigma}_{B,b_1/b_2} \quad \text{for } {}^{D}\tilde{\sigma}_B \gtrsim \sigma_1. \tag{2.3.25} $$

For the case b) it is

$$ \frac{\tilde{\sigma}_B}{{}^{D}\tilde{\sigma}_B} = \left(\frac{b_1}{b_2}\right)^{\frac{1}{n+1}} \tag{2.3.26} $$

and thus

$$ {}^{D}\tilde{\sigma}_B \neq f(\sigma_1) \qquad \text{for } {}^{D}\tilde{\sigma}_B >> \sigma_1. \tag{2.3.27} $$

For the calculation of the life time ${}^{D}\tilde{\tau}_T$ the reader is refered to chapter 2.3.2 .

3. Experimental

In the following a comparison between calculations and experimental data is given. It should be emphasized that most of the experimental results were collected from literature refering to burst tests on Zircaloy tubing. In many cases the informations about the experimental procedure are incomplet. To verify the results of the calculations by systematic experiments, only few results are available at present. These investigations are still going on.

3.1 The Temperature Ramp

In Fig.2 calculated $\tilde{T}_B(c)_{\sigma_0}$-curves are compared with results from burst tests on Zircaloy tubing. For this purpose assuming isotropy the initial pressures $p_{i,0}$ or the hoop stresses respectively have been recalculated to effective tensile stresses using the formula

$$\sigma_{0,eff} = p_i \frac{\sqrt{3}}{2} \frac{R_M}{h}\Bigg|_{t=0} = p_i \alpha \qquad (3.1.1)$$

where R_M is the mean radius and h is the wall thickness.

Results from three laboratories have been considered: BNL(UK) [7], ANL(USA) [8] and KWU(GERMANY) [9].

In all these cases the tubes were ohmically heated. Except the ANL-values there is a rather good agreement for higher heating rates. The KWU-values are mean values for c from an interval of 100 to 150 deg/sec.

According to the results from 2.1.1.3 the discrepancy between e.g. the BNL-results and the calculated ones would indicate, that - under otherwise unchanged conditions - for c=50 deg/sec the actual tubing temperature at burst is lower ($d\tilde{T}_B<0$) and for c=1 deg/sec this temperature is higher ($d\tilde{T}_B>0$) as that predicted by the calculations.

In Fig.5 the experimental life times of blown Zircaloy tubes are compared to calculated ones. Again values from three labs have been used: KWU[9](ohmically heated), IRB[10](internal heater) and IMF[11](radiation heated). The agreement is better for low σ_0-values and high heating rates.

3.2 The Stress Ramp

In Fig.13 results of σ-ramp for tensile tests at b_0=constant are compared to calculations according to Eq(2.1.31). Excellent agreement is observed for the test temperature T_0=1073K. At the other temperatures examined there are for $b \gtrsim 1$MPa/sec deviations from the predicted results. The influence, recrystallization has upon $\tilde{\sigma}_B$ is clearly demonstrated by comparing the results from as-received samples with those from recrystallized ones. However there is still a deviation for the recrystallized specimens which manifests the occurrence of dynamic recrystallization during the σ-ramp test. This is not observed for T_0=1073K which is above the region of recrystallization. We will return to this point in chapter 4.2.

4 Discussion

4.1 Model Considerations

From the comparison of ramp calculations with experiments (chapter 3) it is obvious, neglecting the explanable influence of recrystallization, that the LFR is obeyed for Zircaloy in the temperature range between 600°C and 800°C. In this range Zircaloy fails in ductile manner[12]. Metallographic investigations on specimens deformed at the above conditions gave evidence about abundant cavitation[13] which in the present case is to be considered as the specific damage type leading to fracture. Previous examinations habe shown[14] that grain boundary sliding becomes the dominant deformation mechanism at the α/α+β phase boundary. This mechanism is known as being mainly responsible for cavity nucleation[15].

RAJ and ASHBY [16] developed a model which allows to calculate the time to intercrystalline fracture on the basis of considerations about nucleation and growth of voids in grain boundaries. From the model it follows that the life time τ under otherwise unchanged conditions is a function of stress and temperature only. Due to the model fracture occurs as the consequence of the reduction of the internal cross section at a critical damage

$$A_f = \left(\frac{R_B}{L}\right)^2_f \qquad (4.1.1)$$

where R_B is the projection of the void radius into the grain boundary and 2L is the distance of the voids in a square array. Using this model for the present case we assume that for the damage rate $\dot{A} = \frac{dA}{dt}$ at iso-conditions the proportionality holds

$$\dot{A} = \frac{1}{\tau} A(t)_{\sigma,T,\phi} \qquad (4.1.2)$$

where the "structure" parameter ϕ can include e.g. also the void distance L. From the above it follows that

$$\left.\frac{dA}{A(t)}\right|_{\sigma,T,\phi} = \left.\frac{dt}{\tau}\right|_{\sigma,T,\phi} \qquad (4.1.3)$$

Considering non-steady loading conditions we obtain from Eq(4.1.3) and by comparison with Eqs.(2.1.2) and (2.1.27) respectively

$$\int_{t_0}^{\tilde{\tau}} \frac{dA}{A(\sigma,T,t)_\phi} = \int_{t_0}^{\tilde{\tau}} \frac{dt}{\tau(\sigma,T,t)_\phi} = 1 \; . \qquad (4.1.4)$$

Eq(4.1.4) says, that at constant "structure" failure under variable stress and temperature will occur at the time $\tilde{\tau}$ when at

that time the "damage integral"

$$\int_{t_0}^{\tilde{\tau}} \frac{dA}{A(\sigma,T,t)_\phi} \equiv \Lambda_A\,(\sigma,T)_\phi = 1 \qquad (4.1.5)$$

Eq(4.1.5) can thus be considered as a definition of the life time of materials subjected to general loading conditions. When failure would occur by the growth of voids at constant void density, it follows from Eqs.(4.1.1) and (4.1.3) for Λ_A

$$1 = \Lambda_A(\sigma,T)_{\phi,L} = 2\int_{R_B(t_0)}^{R_B(\tilde{\tau})} \frac{dR_B}{R_B(\sigma,T)_{\phi,L}} \,. \qquad (4.1.6)$$

For the case considered the experimental determination of $R_B(t)$ would principally allow to check the model.

The parameter ϕ plays an important role. ϕ is specified by material properties which are important for the nucleation and growth of voids in the grain boundaries. Therefore one can expect that processes which involve grain boundaries will influence the life time sensitively.

This can be illustrated by the following consideration. Suppose that for a material which is σ-ramped the damage at the time t is $A_1(t,\phi)$. The damage will change by time.

For ϕ=const. this change will be at t+dt $dA_1(dt)\phi$. This corresponds to the shift of point O in the Å-A diagram (see Fig.14) along the curve

$$\dot{A}_1 = \frac{1}{\tau_1} A_1 \qquad (4.1.7a)$$

to position 1. If now the s t r u c t u r e w i l l c h a n g e by time in a way that $dA_1(dt)_\phi$ and $dA'_1(d\phi)_{dt}$ simply superimpose, the damage is characterized in Fig.14 by $dA'_1(dt,d\phi)$. The damage $A'_1=A_1+dA'_1$ may be represented in Fig. 14 by 1'. The change in damage now occurs along another $\dot{A}_1(A)$ curve e.g.

$$\dot{A}'_1 = \frac{1}{\tau'_1} A'_1 \qquad (4.1.7b)$$

According to Eq(4.1.2) it follows from Fig.14 that

$$\tau'_1 > \tau_1 \qquad (4.1.8)$$

due to Eq(4.1.3) it is

$$\int \frac{dA_1}{A_1} = \int \frac{dt}{\tau_1} \qquad (4.1.9a)$$

and

$$\int \frac{dA'_1}{A'_1} = \int \frac{dt}{\tau'_1} \qquad (4.1.9b)$$

Applying the LFR to the Eqs.(4.1.9a) and (4.1.9b) respectively, we obtain

$$\int_{t_0}^{\tilde{\tau}_1} \frac{dt}{\tau_1} = \int_{t_0}^{\tilde{\tau}'_1} \frac{dt}{\tau'_1} = 1 \qquad (4.1.10)$$

Because according to Eq(4.1.8) the infinitesimal contributions are smaller for the integral on the right hand side of Eq(4.1.10), it necessarily follows from Eq(4.1.10) that

$$\tilde{\tau}'_1 > \tilde{\tau}_1 \qquad (4.1.11)$$

Suppose that $A = A(R_B, L)_\phi$, so that

$$dA = \left\{\frac{\partial A}{\partial R_B}\right\}_L dR_B + \left\{\frac{\partial A}{\partial L}\right\}_{R_B} dL \qquad (4.1.12)$$

applying this to the case considered, $d\phi=0$ would mean that A_1 has changed by increasing the void radius R_B at L=constant. In this case

$$dA_1 = \left\{\frac{\partial A_1}{\partial R_B}\right\}_L dR_B \ . \qquad (4.1.13)$$

On the other hand, if dA_1' is caused by a change in R_B as well as in the void concentration, we have

$$dA_1' = \left\{\frac{\partial A_1'}{\partial R_B}\right\}_L dR_B + \left\{\frac{\partial A_1'}{\partial L}\right\}_{R_B} dL \qquad (4.1.14)$$

From Eq(4.1.1) it follows that

$$\left\{\frac{\partial A}{\partial R_B}\right\}_L = \frac{2R_B}{L^2} \qquad (4.1.15a)$$

and

$$\left\{\frac{\partial A}{\partial L}\right\}_{R_B} = -\frac{2R^2}{L^3} \qquad (4.1.15b)$$

From Fig.14 it is

$$dA_1' - dA_1 > 0 \qquad (4.1.16)$$

Combining the Eq(4.1.13)(4.1.14)(4.1.15) and (4.1.16) we obtain

$$dA_1' - dA_1 = -2A_1\frac{dL}{L} > 0 \qquad (4.1.17)$$

consequently

$$dL < 0 \ . \qquad (4.1.18)$$

Thus according to the model the change in ϕ considered would be due to an increase in void concentration. However, for a given value $dA_1' - dA_1$ the change $dL<0$ could be very small providing the damage A_1 and the concentrations of voids are high enough.

It has been already emphasized that, before using the results of calculations for predictions the validity of the LFR for each particular case should be checked experimentally. In the following we consider some very general aspects for the design of such experiments.

From the consideration above about the influence of ϕ in the experiments proposed, test conditions should be rejected which would lead to a change of those "structure"-factors influencing sensitively the life time, as in the present case e.g. recrystallization, grain growth, precipitation on grain boundaries as well as solution of precipitates, generation of radiation defects et cet.

Also the influence of the duration of the test is easily realized. One of the assumptions of the LFR is based upon the mutual dependency of the life time fractions. Using the concept of damage fractions (see Eq(4.1.3)) this independency means that e.g.the damage $A(T_1)$ the sample had at T_1 has not been influenced by the deformation at the higher temperatures $T_1 > T_1$. This could happen e.g. by annealing. Consequently for checking the validity of the LFR fast ramp tests seem more appropriate than a test procedure using finite stress or temperature steps.

Treating the case of superimposed ramps (chapter 2.2) the individual contributions of the T- and σ-ramp habe been considered as mutually independent. In the following we will try to get arguments for this assumption from the model.

From the Eq(4.1.12) it is

$$\frac{dA}{A} = \frac{1}{A(\sigma,T)_{t,\phi}} \left(\frac{\partial A}{\partial \sigma}\right)_{T,t,\phi} \cdot d\sigma + \frac{1}{A(\sigma,T)_{t,\phi}} \left(\frac{\partial A}{\partial T}\right)_{\sigma,t,\phi} \cdot dT \qquad (4.1.19)$$

which, assuming the validity of the LFR leads by using Eq(4.1.2)

to

$$\int_{t_0}^{\tilde{\tau}} \frac{dA}{A(\sigma,T,t)_{\phi}} = \int_{t_0}^{\tilde{\tau}} \frac{dt}{\tau(\sigma,T,t)_{\phi}} = 1 \qquad (4.1.20)$$

and therefrom

$$\frac{d}{dA} \int_{t_0}^{\tilde{\tau}} \frac{dA}{A} = \frac{dA}{A} = 0 \; . \qquad (4.1.21)$$

Combining Eqs.(4.1.19)(4.1.20) and (2.2.1) one obtains

$$\tau[T(t)]_{\sigma,\phi} = \frac{A[T(t)]_{\sigma,\phi}}{c\left\{\frac{\partial A}{\partial T}\right\}_{\sigma,\phi}} \qquad (4.1.22a)$$

and

$$\tau[\sigma(t)]_{T,\phi} = \frac{A[\sigma(t)]_{T,\phi}}{b\left\{\frac{\partial A}{\partial \sigma}\right\}_{T,\phi}} \qquad (4.1.22b)$$

comparing Eqs.(4.1.22) with Eq(4.1.2) it is

$$\dot{A}(T)_{\sigma,\phi} = c\left(\frac{\partial A}{\partial T}\right)_{\sigma,\phi} \qquad (4.1.23a)$$

and

$$\dot{A}(\sigma)_{T,\phi} = b\left(\frac{\partial A}{\partial \sigma}\right)_{T,\phi} \qquad (4.1.23b)$$

where $\left(\frac{\partial A}{\partial T}\right)_{\sigma,\phi}$ and $\left(\frac{\partial A}{\partial \sigma}\right)_{T,\phi}$ are properties of a given damage structure.

Thus from the model the validity of Eq(2.2.1) depends on whether Eq(4.1.2) and the LFR are obeyed. Or equivalently, if the validity of the Eq(2.2.1) should be confirmed by experiments, this would confirm the validity of Eq(4.1.2) and that of the LFR. In this case the damage $A(\sigma,T)_{\phi}$ would behave as a function of state (see Eq(4.1.21)).

4.2. Applications to Zircaloy

As already mentioned the stimulus to this work was given by the problem to predict the failure of fuel pins in LWR's subjected to the conditions of a hypothetical LOCA. Therefore at present the application of some of the results of the preceding calculations to Zircaloy will be briefly discussed. In the following we restrict the considerations to the α-phase region to preclude the difficulties appearing in cases with non constant structure parameter ϕ (see chapter 4.1). The lower boundary of the temperature range under consideration is given by the temperature at which the contribution of life time fractions is practically notable. For the stress range of interest this temperature turned out to be approximately 873K. In the following a brief list of data is given which were used for the present calculations [11].

Temperature [K]	n
873	7,1
973	6,3
1073	5,2

$$\frac{Q}{R} = 3.75 \times 10^4 [K]$$

$$P = \frac{Q}{RT_0} \qquad (2.1.4)$$

α $\frac{MPa}{bar}$ in Eq(3.1.1)	Cladding type:
1.51	CANDU (CANADA)
0.95	SGHWR (UK)
0.70	ANL (USA)
0.59	KWU (F.R.GERMANY)
0.49	BETTIS (USA)

The T_0 -values which correspond to given T_0 - and σ_0 -values are obtained from the stress rupture diagram in Fig.1. All the data were determined from vacuum tensile tests on Zircaloy-4.

4.2.1 Failure Prediction

The occurence of failure has to be predicted for known loading conditions. As an example we consider cladding which, starting from normal in-pile operating conditions, is subjected to very fast superimposed ramps.

R a m p c o n d i t i o n s :

$\sigma_0^{\ast}$(723K) $\doteq$ 2bar $\triangleq$ 1,2MPa UNIAXIAL
$T_0^{\ast}$ = 723 K — initial conditions

Duration of the ramp t_D = 5sec

σ_{max} = 60bar $\triangleq$ 35,4MPa UNIAXIAL
T_{max} = 1113K — final conditions
c,b = const. $\neq$ f(t).

From these conditions it follows that
c = 48 deg/sec and
b = 6,8Mpa/sec .

Consider the situation at the lowest relevant temperature T_0=873K.

$$\sigma_0(873K) = \sigma_0^{*} + bt_x$$

$$T_0 = 873K = T_0^{*} + ct_x$$

thus

$$\sigma_0(873K) = \sigma_0^{*} + \frac{b}{c}(T_0 - T_0^{*}) = 22{,}2MPa$$

From Fig.1 it is for T_0=873K and σ_0=22,2MPa

$$\tau_0 = 7x10^{6}sec$$

For orientation we check the condition given by Eq(2.2.4) and compare the ratio

$$\frac{\sigma_0}{s_{\tilde{T}_B} - T_0} = 9.25 \times 10^{-2}$$

to

$$\frac{b}{c} = 1.4 \times 10^{-1} \gtrsim \frac{\sigma_0}{s_{\tilde{T}_B} - T_0}$$

It follows from the calculations in chapter 2.2 that in this case the σ-ramp can not be neglected in the superimposed ramp. The present case therefore has to be treated by means of Eq(2.2.8).

Inserting the above values together with P=43 and n=7,1 in Eq(2.2.8) and putting $s_{\tilde{T}_B}=T_{max}$ (assumption, that failure occurs at T_{max}), one obtains

$$\left(\frac{c}{b}\right)_{cal.} \doteq 1{,}3 \times 10^{-8}$$

This result compared to the actual ramp condition

$$\left(\frac{c}{b}\right)_{exp.} = 7{,}1$$

means that under the given conditions failure will not occur. To obtain fracture at T_{max} the stress rate b has to be increased, assuming c as fixed, at least by seven orders of magnitude. This would correspond to an extrem impact loading.

On the basis of Eq(2.2.4) a line is shown in Fig.15 which,for a given σ_0-value and given temperature difference, divides the (b,c)-plane so that points above this line represent the situation when in the superimposed ramp the σ-ramp is important, the points below the line when the σ-ramp does not influence the result of the T-ramp.

4.2.2 Comparison to Experiments

In modelling the inelastic behavior of fuel rods in LWR's under off-normal conditions it is important to know the rupture stress $\tilde{\sigma}_B$. In the past a lot of data were collected [2] to allow for the prediction of burst behavior of Zircaloy cladding on an empirical basis. These results, usually represented in the form of Fig.2, exhibit considerable scatter which in turn increases the conservatism of the predictions.

In the calculated curves in Fig.2 which correlate the initial stress σ_0 with $\tilde{T}_B$ in a T-ramp test the stress σ_0 can be replaced by the burst stress ${}^s\tilde{\sigma}_B$ so far as for a superimposed ramp the condition given by Eq(2.2.4) is obeyed. If this condition is not obeyed, the ${}^s\tilde{\sigma}_B$-values can be calculated by means of Eq(2.2.8) from the ${}^s\tilde{T}_B$-values using (2.2.2a). All the stresses considered in the paper up to now are n o m i n a l stresses. The prediction of the true burst stress ${}^s\tilde{\sigma}_{B,T}$ is due to the wellknown difficulties generally not possible.

It is the advantage of the calculations that they allow to understand the $\sigma_0(\tilde{T}_B)$-dependence and to explain the influence of the ramp conditions on that dependence. As was already emphasized in chapter 2.1.1.3 the deviations of the experimental values from the predicted ones could be due to the difference between the m e a s u r e d temperature $\tilde{T}_B(M)$ and the temperature $\tilde{T}_B$ for which the location of the particular point $(\sigma_0, \tilde{T}_B)_c$ in Fig.16 was calculated.

To confirm this T-ramp tests have been conducted on Zircaloy-4 tensile specimens in vacuum[10]. The material was crept under constant load in an INSTRON machine and radiation heated at constant rates c. The temperature measurement was performed by a

thermocouple located close to the surface of the specimen. The results of these experiments together with the calculated curves are shown in Figs.16 and 17.

There is very good agreement between experiments and calculations, for low heating rates the deviation increases with increasing heating rate. As explained in chapter 2.1.1.3 for the deviation temperature differences may be responsible. This can be easily understood by means of Fig.16.
Each point on the calculated $\sigma_0(\tilde{T}_B)_c$-curves is for a given σ_0- and c-value determined by the corresponding $\tilde{T}_B$-value. It is acceptable to assume that accurate σ_0- and c-values are maintained experimentally easier than it is possible to determine the a c t u a l temperature of failure $\tilde{T}_B$ of the samples. Thus in the present case demonstrated in Fig.16 one can expect that for samples heated by radiation the a c t u a l temperature will be generally lower as that measured by the thermocouple. Further, this difference should increase with increasing heating rate. On the basis of the Eqs.(2.1.23) the experimental values can be corrected for this temperature difference.

The correction in Fig.16 and 17 respectively was performed in the following way. For given σ_0- and c-experimental values the temperature change $d\tilde{T}_B$ was determined as the difference $\tilde{T}_{B,exp.} - \tilde{T}_{B,cal.}$ between the measured and calculated $\tilde{T}_B$-values. Together with $\tilde{T}_{B,cal.}$ and σ_0 the value $d\tilde{T}_B$ was inserted into Eq(2.1.23b) and therefrom $d\sigma_0$ was calculated. As one can realize from Fig.16 and 17 this correction in general improves the fit between the experiments and calculations.

The experimental values in Fig.2 have been obtained on ohmically heated cladding. Contrary to the case mentioned above no large temperature differences are expected in this case especially when the temperature was measured pyrometrically (see KWU-results). Note that the deviations of $\tilde{T}_{B,exp.}$ from the calculated $\tilde{T}_B$-values behave in a way as predicted by Eq(2.1.25). However, the ANL-results deviate heavily from the predictions.

Finally the excellent reproducibility of the results of the preliminary σ- and T-ramp tensile tests should be emphasized. The reproducibility turned out to be substantially better than that well known from iso-stress rupture tests.

4.3 General Conclusions

From this comparison the substantial conclusion follows that for Zircaloy in the particular range of conditions examined the LFR is obeyed.

Complications appear when recrystallization comes into the play. On the basis of a quite general consideration in chapter 4.1 this is unterstood principally.

According to the model of RAJ and ASHBY [16] -which forms the basis of these considerations the d u c t i l e i n t e r - c r y s t a l l i n e f a i l u r e is governed by mechanism which in general is different from those responsible for the plastic strain. Consequently a causal link between time to rupture and strain at failure ε_B is not expected to exist in this case.

5. Summary

1. On the basis of the life fraction rule the rupture time and the correlated failure stress and failure temperature respectively for several monotoneous ramp loading conditions have been calculated. The results are expressed by iso-stress rupture data and by the particular loading conditions.
Thus the results of ramp rupture test can be predicted from rupture tests conducted at constant load and temperature respectively, without any fitting procedure.

The sensitivity of the results to variations of test parameters are examined. This enables a profound analysis of the experimental data.

For the special and practical important case where σ- and T-ramps are superimposed-depending on the rate ratio $\frac{b}{c}$ - between two cases can be distinguished. For low stress rates b the T-ramp is dominating whereas for high b-values both the ramps influence the result.

2. The life fraction rule has been checked for Zircaloy-4 comparing the results of ramp-rupture tests with calculations. Excluding conditions when dynamic recrystallization interferes, the LFR is obeyed for the temperature range 600-840 °C. These deviations can be understood by means of a damage model.

3. The discussion of the LFR is based on the model developed by RAJ and ASHBY for ductile intercrystalline failure. It is shown that the LFR is obeyed as far as the appropriate damage function $A(T,\sigma)_\phi$ behaves as a function of state.

Aknowledgement

I wish to thank Mr.C.Petersen and Mr.S.Raff for valuable comments and support. To Mr.H.Schneider I am indebted for performing the experiments. This work was supported by the Nuclear Safety Project of the Kernforschungszentrum Karlsruhe through the contract Projekt Nukleare Sicherheit 06.01.06/01A.

List of Figures

Fig. 1 Stress rupture curves.

Fig. 2 The T-ramp. The temperature at failure vers. stress (the calculations are represented by lines).

Fig. 3 The T-ramp. The life time vers. heating rate (calculated from Eq(2.1.9)).

Fig. 4 The T-ramp. The temperature at failure vers. heating rate (graph of the function given by Eq(2.1.9)).

Fig. 5 The T-ramp. The life time as a function of stress (the calculations are represented by lines).

Fig. 6 The σ-ramp. The normalized stress at failure vers. stress rate (graph of the function given by Eq(2.1.33)).

Fig. 7 The σ-ramp. The normalized equivalent stress at failure vers. $\frac{\sigma_0}{b\tau_0}$.

Fig. 8 Superimposed ramps.

Fig. 9 Superimposed ramps. The dependence of ${}^{s}\tilde{T}_B$ on the rate ratio $\frac{c}{b}$ (see Eq(2.2.8)).

Fig.10 The T-ramp-hold procedure.

Fig.11 The σ-ramp-hold procedure.

Fig.12 The double T-ramp.

Fig.13 The σ-ramp. The stress at failure vers. stress rate (calculations are represented by solid lines).

Fig.14 The damage function (see text).

Fig.15 Superimposed ramps (graphical representation of the criterion given by Eq(2.2.4)).

Fig.16 The T-ramp. The temperature at failure vers. stress. Correction of experimental values for temperature differences (calculation represented by solid lines).

Fig.17 The T-ramp. The life time vers. stress. Correction of experimental values for temperature differences (calculations represented by solid lines).

Literature

[1] S.Tayra, "Creep in Structures", Springer, Berlin-Göttingen-Heidelberg, 1962, p.96.

[2] Proceedings of Specialist Meeting on"The Behavior of Water Reactor Fuel Elements under Accident Conditions", Spåtind, Norway,13.-16.th of September 1976, CSNI Report No.13, Vol.I,II.

[3] E.L.Robinson, Trans.Asme 60, 253 (1938).

[4] B.Ilschner,"Hochtemperaturplastizität",Springer, Berlin-Heidelberg-New York, 1973

[5] H.Böhm and C.Wassilew,"Fuel and Fuel Elements for Fast Reactors",IAEA, Vienna 1974, Vol.II, p.169.

[6] K.D.Closs, "Untersuchungen zum Zeitstand- und Kriechverhalten des Stahls X8CrNiMoVNb1613, Ws.1.4988 bei konstanter und wechselnder Temperatur", KfK-Report 2112, 1975.

[7] B.D.Clay, T.Healey and G.B.Redding, see [2] , Vol.I, Session 1 , Paper No.9.

[8] H.M.Chung, A.M.Garde, E.I.H.Lin and T.F.Kassner, ANL-76-15, 1975, p.53

[9] G.Cheliotis and H.G.Weidinger,"Sicherheitsaspekte beim LWR-Brennstab",1976, p.25, ed. S.B.I.Krawczynski and B.Hürttlen.

[10] F.Erbacher, H.J.Neitzel and K.Wiehr, July 1978, (unveröffentlicht).

[11] M.Boček et al., to be published.

[12] H.M.Chung, A.M.Garde and T.F.Kassner, ANL-76-121, 1976, p.81.

[13] M.Boček and C.Petersen, to be presented at the ANS 1978 Winter Meeting, Washington D.C., November 12-17, 1978.

[14] M.Boček, P.Hoffmann and C.Petersen,"Zirconium in the Nuclear Industry",ASTM 633, 1977, p.66.

[15] B.Burton, Phil.Mag., 30, 953(1974)

[16] R.Raj and M.F.Ashby, Acta Met, 23, 653(1975)

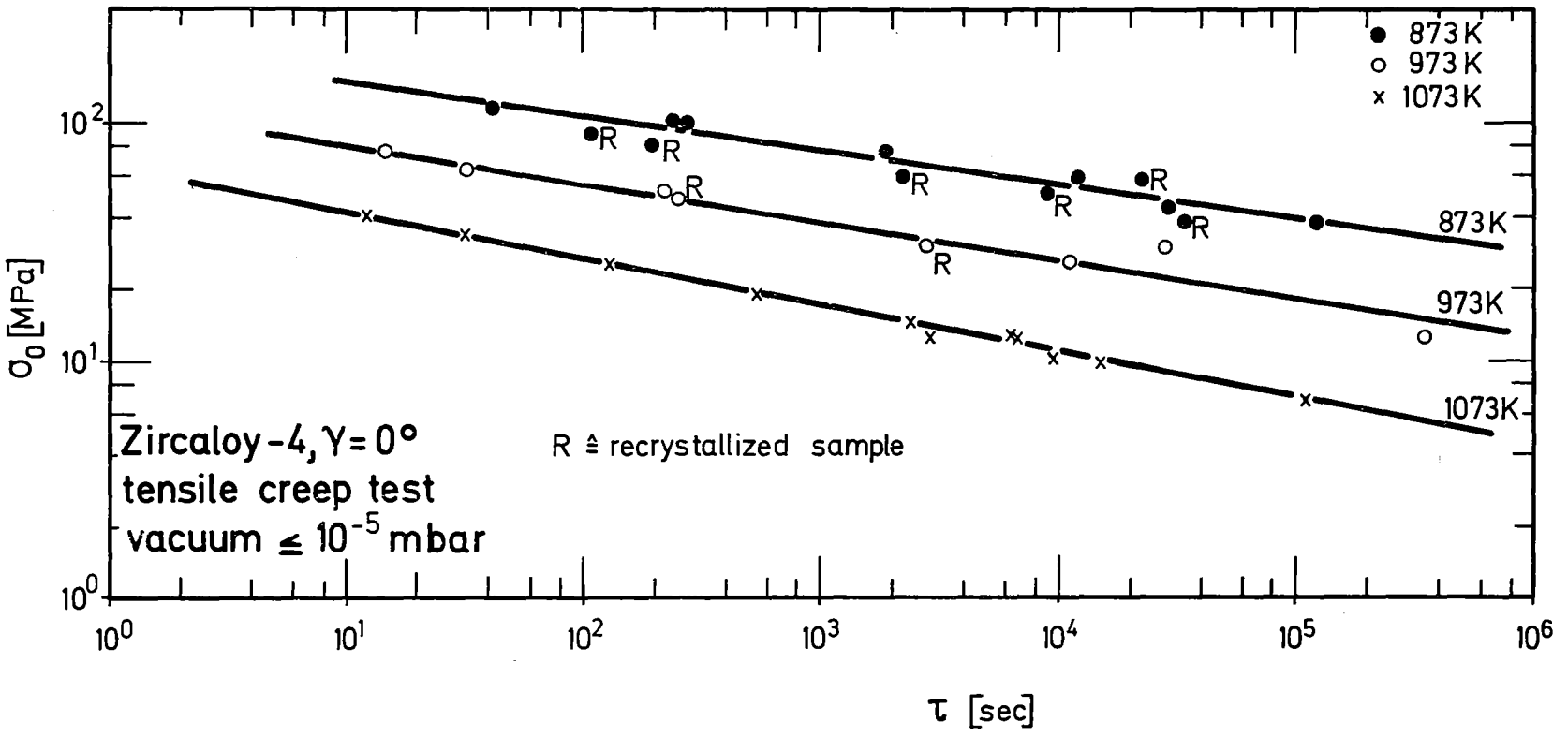

Fig. 1 Stress rupture curves.

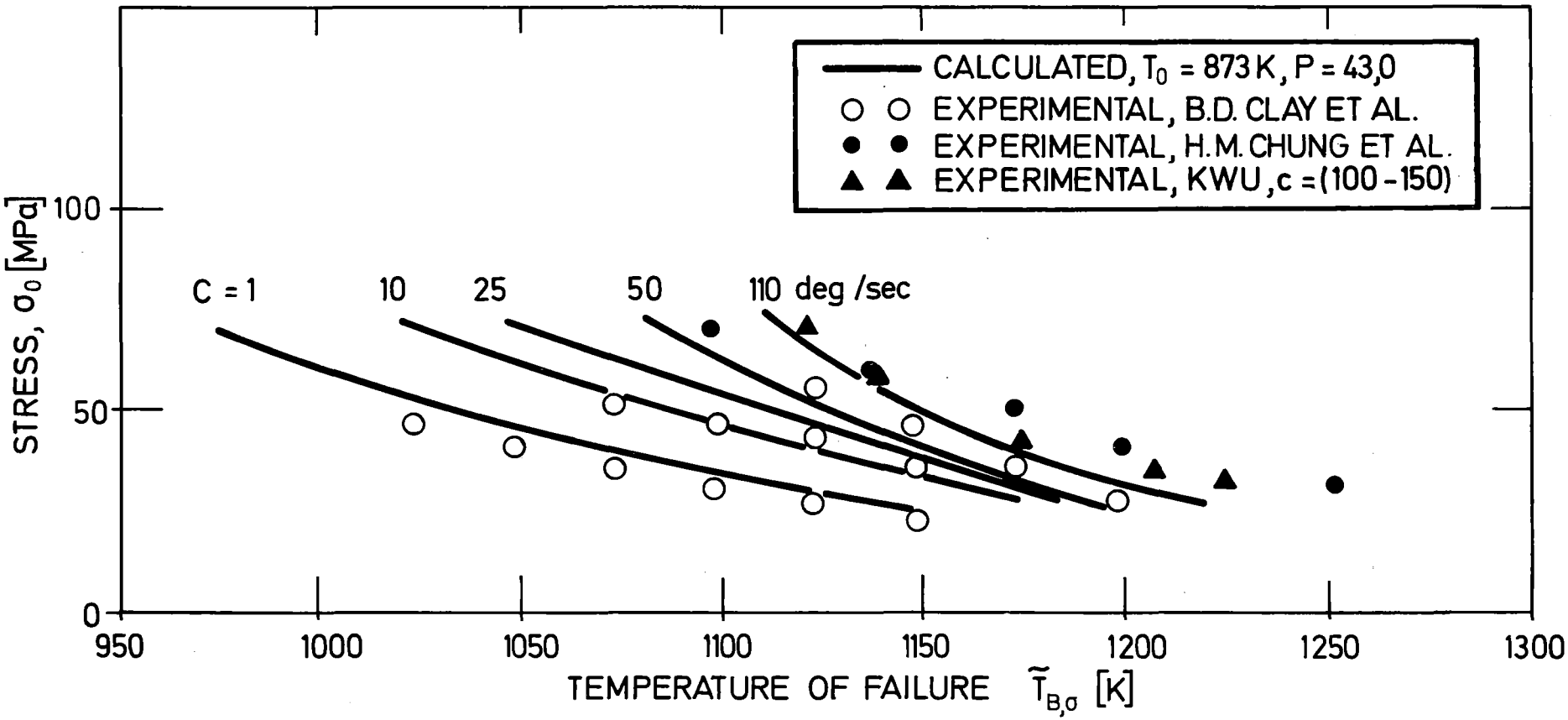

Fig. 2 The T-ramp. The temperature at failure vers. stress (the calculations are represented by lines).

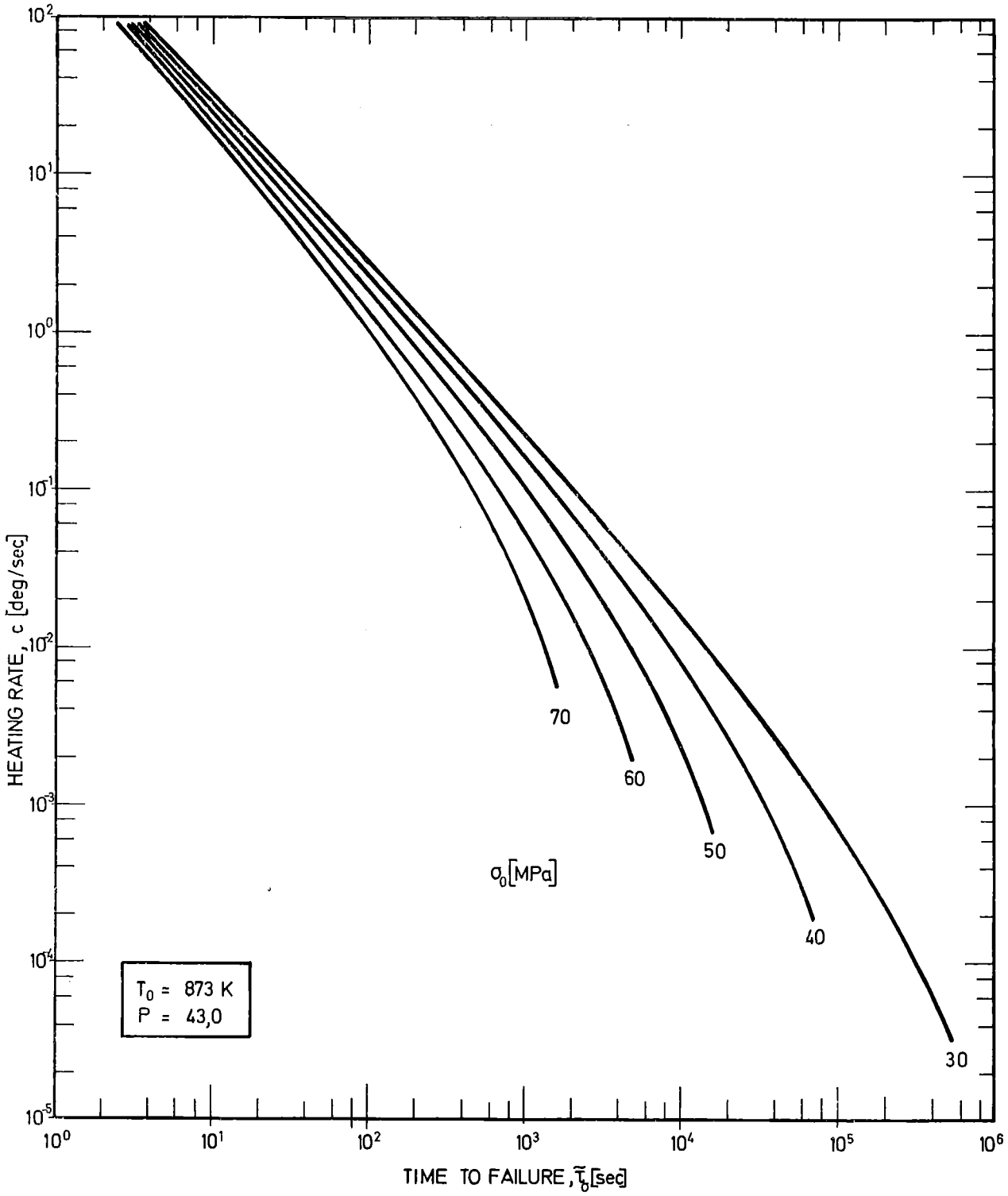

Fig. 3 The T-ramp. The life time vers. heating rate (calculated from Eq(2.1.9)).

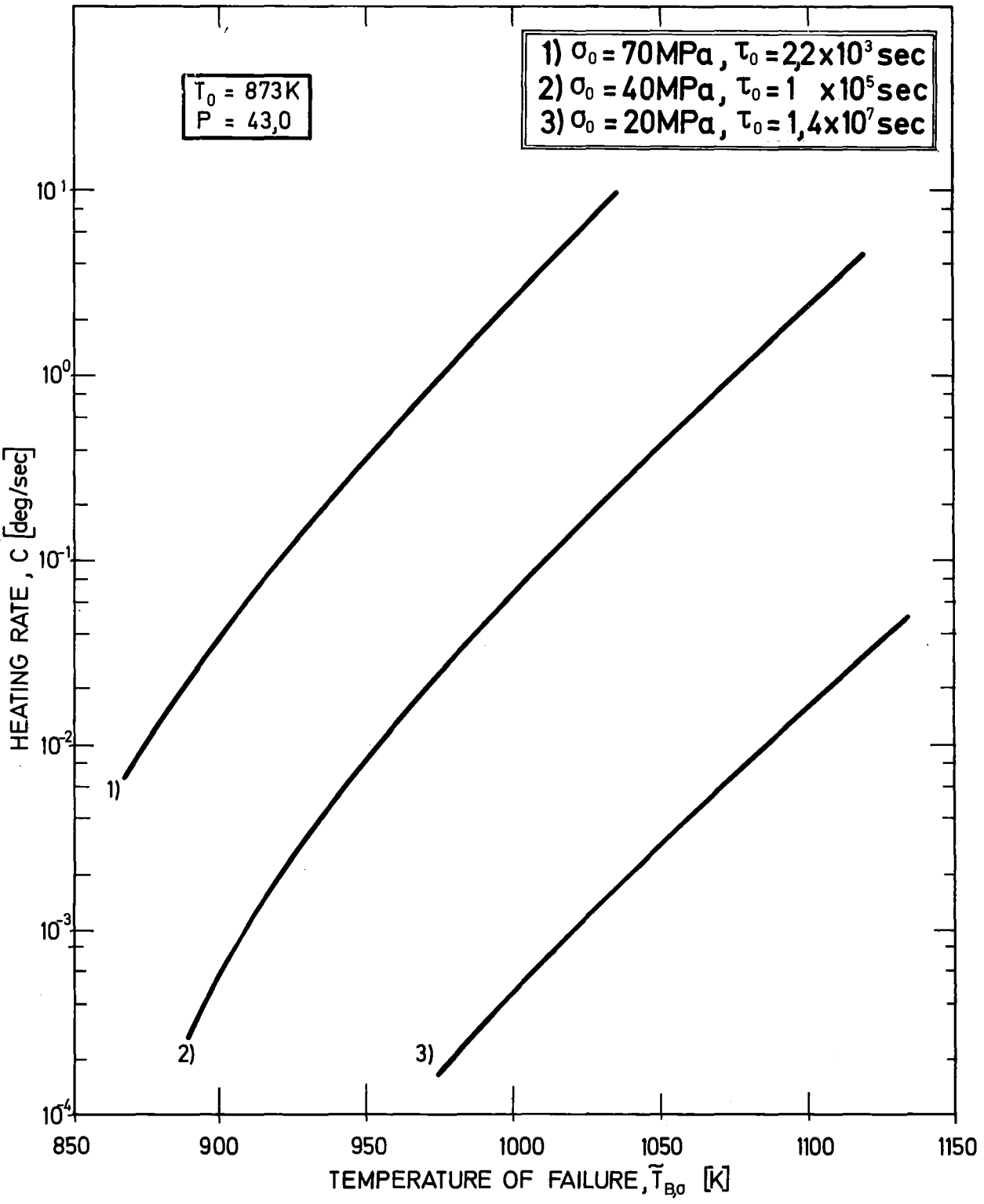

Fig. 4 The T-ramp. The temperature at failure vers. heating rate (graph of the function given by Eq(2.1.9)).

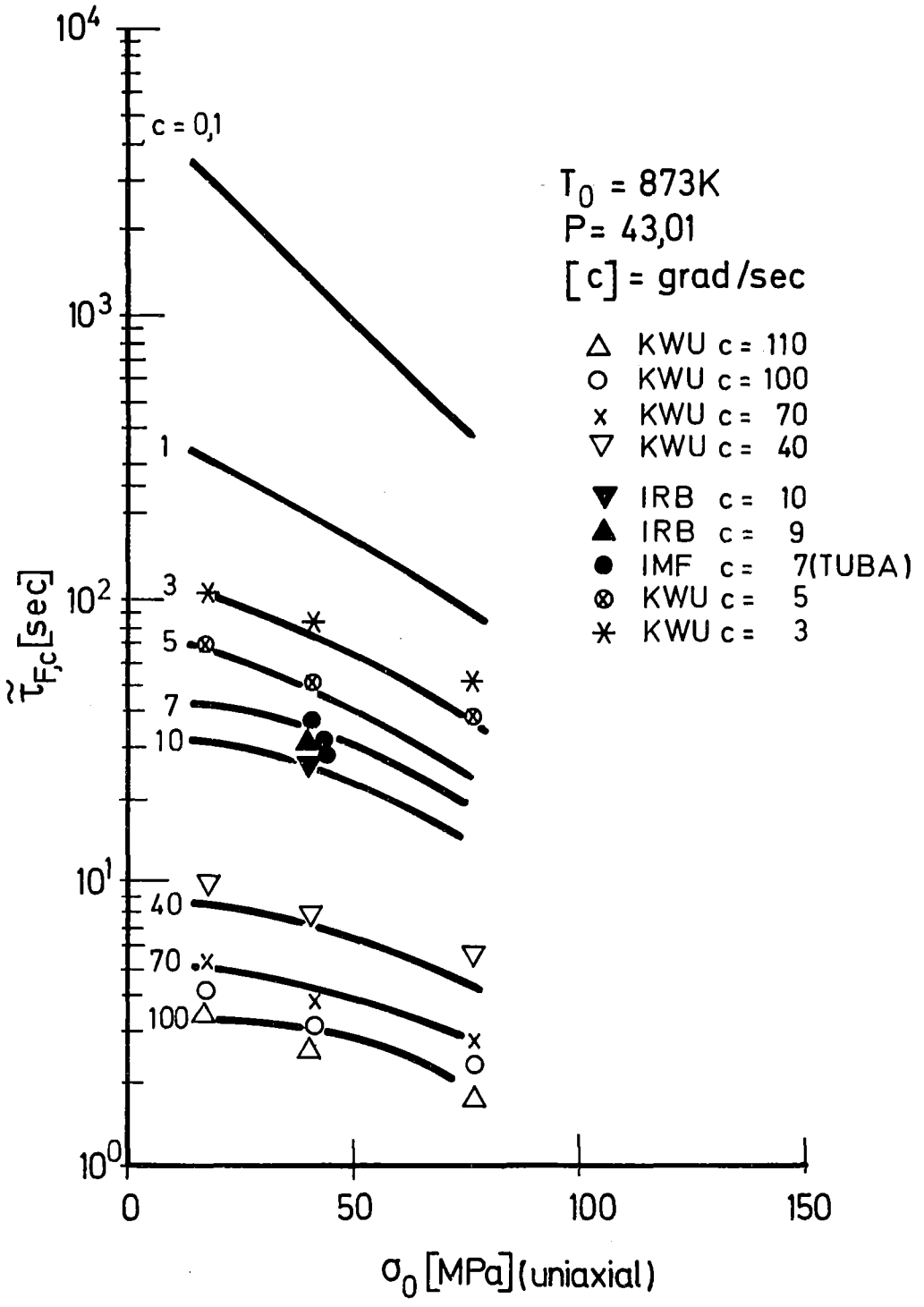

Fig. 5 The T-ramp. The life time as a function of stress (the calculations are represented by lines).

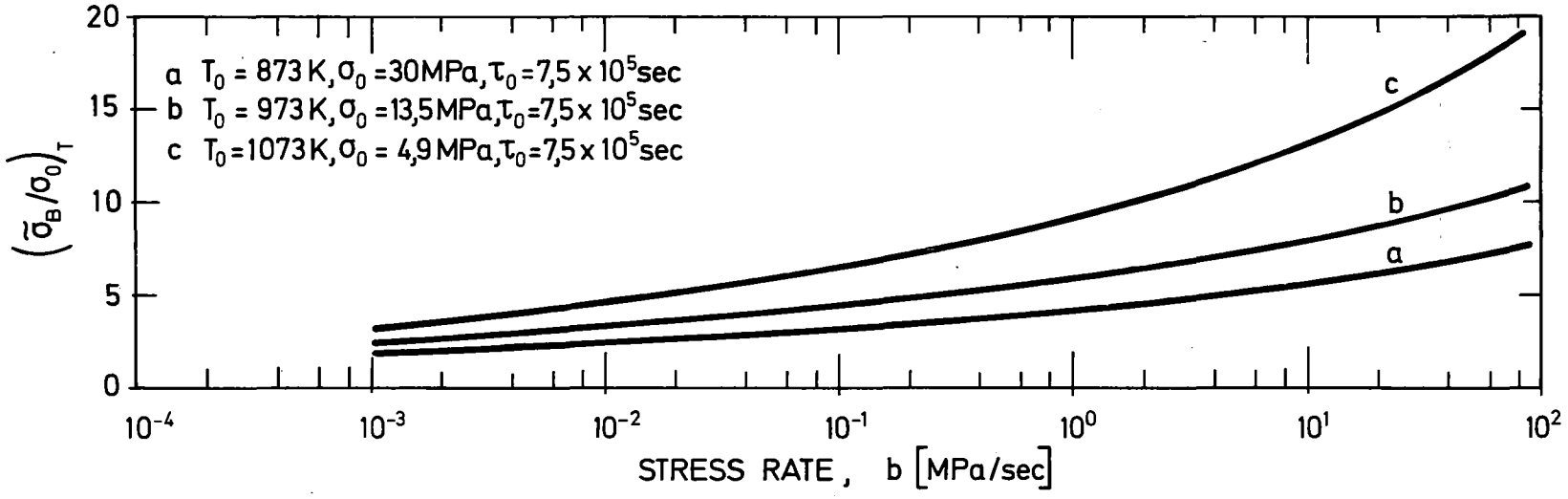

Fig. 6 The σ-ramp. The normalized stress at failure vers. stress rate (graph of the function given by Eq(2.1.33)).

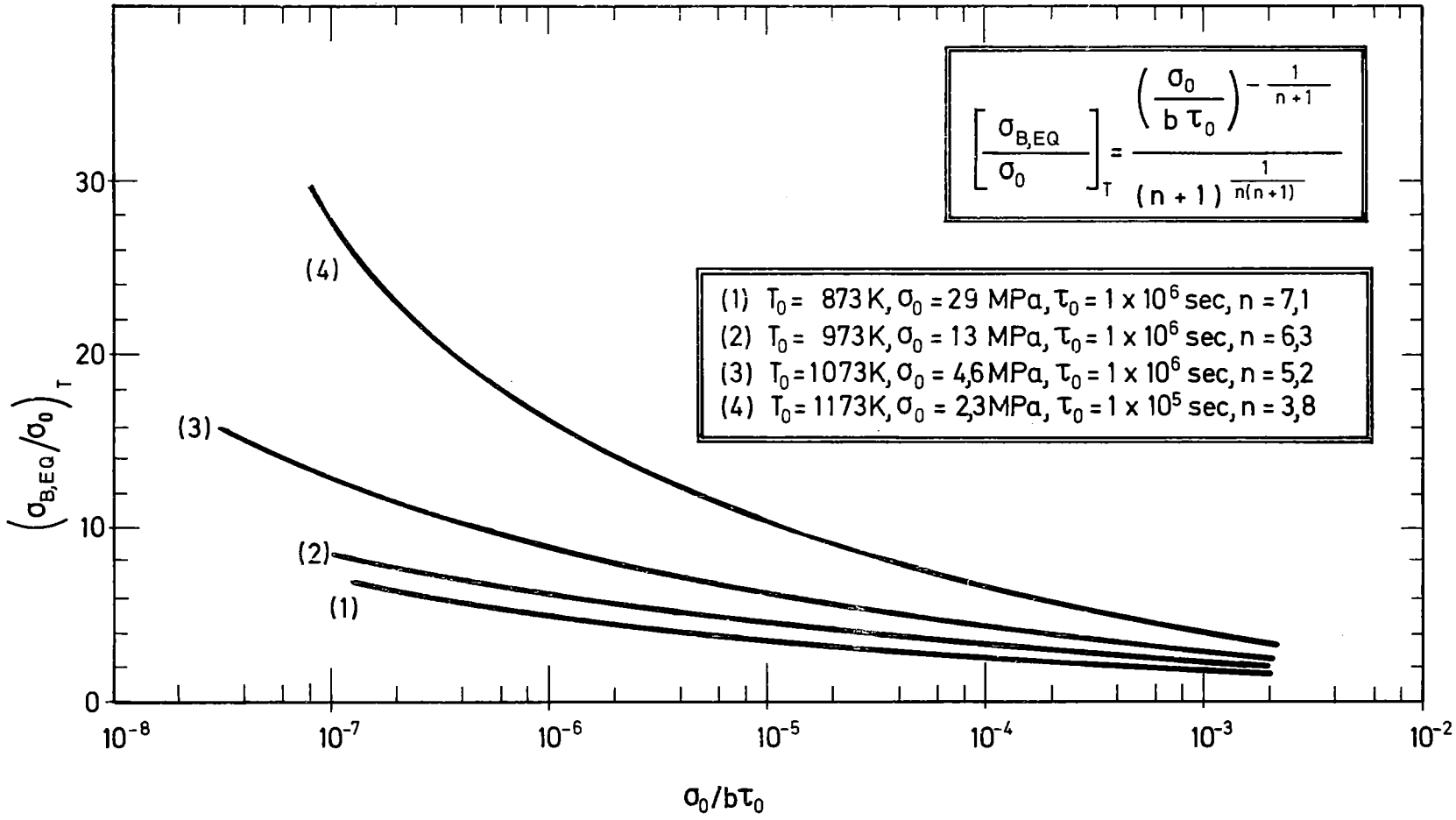

Fig. 7 The σ-ramp. The normalized equivalent stress at failure vers. $\frac{\sigma_0}{b\tau_0}$.

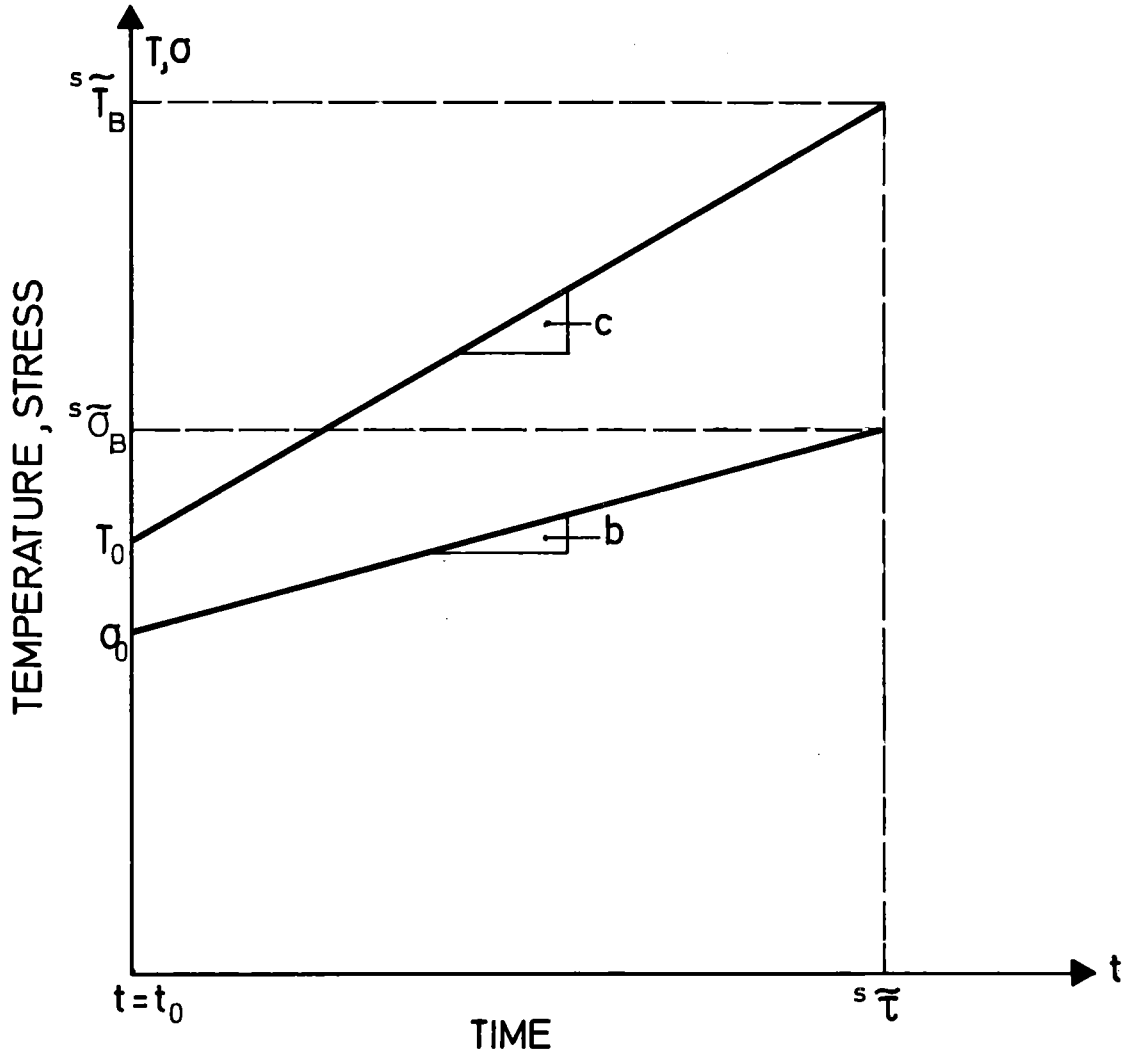

Fig. 8 Superimposed ramps.

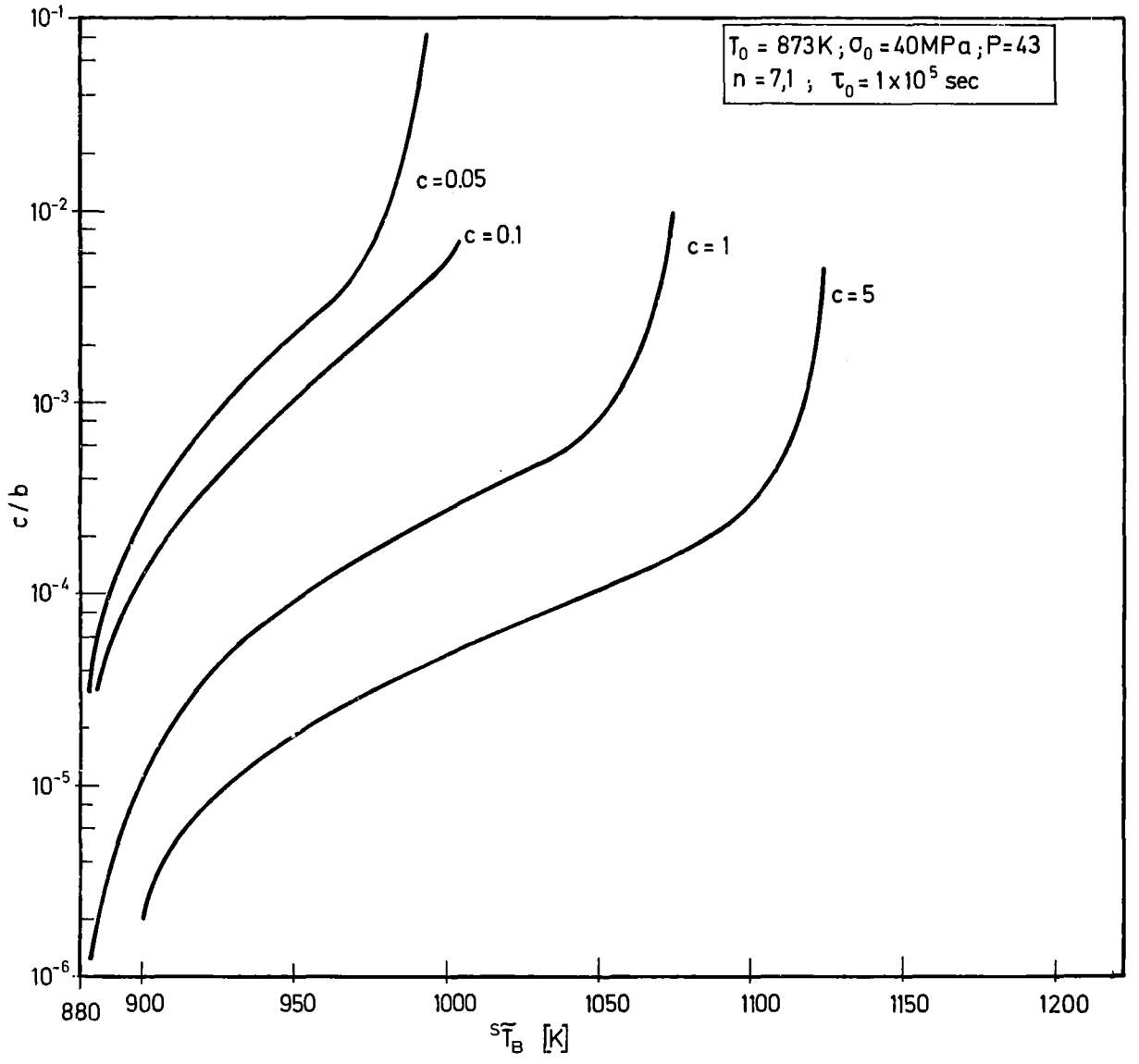

Fig. 9 Superimposed ramps. The dependence of $^s\tilde{T}_B$ on the rate ratio $\frac{c}{b}$ (see Eq(2.2.8)).

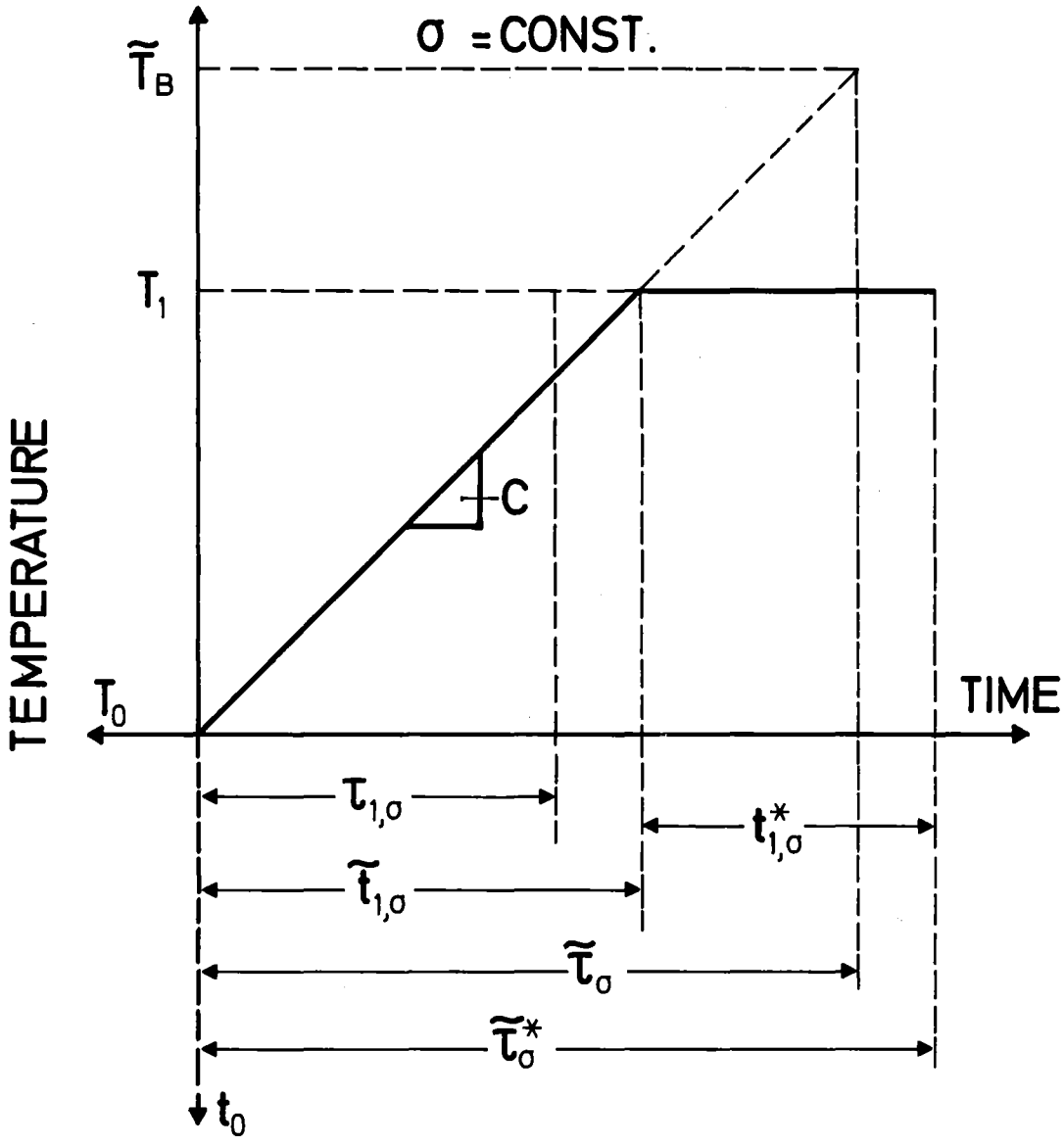

Fig.10 The T-ramp-hold procedure.

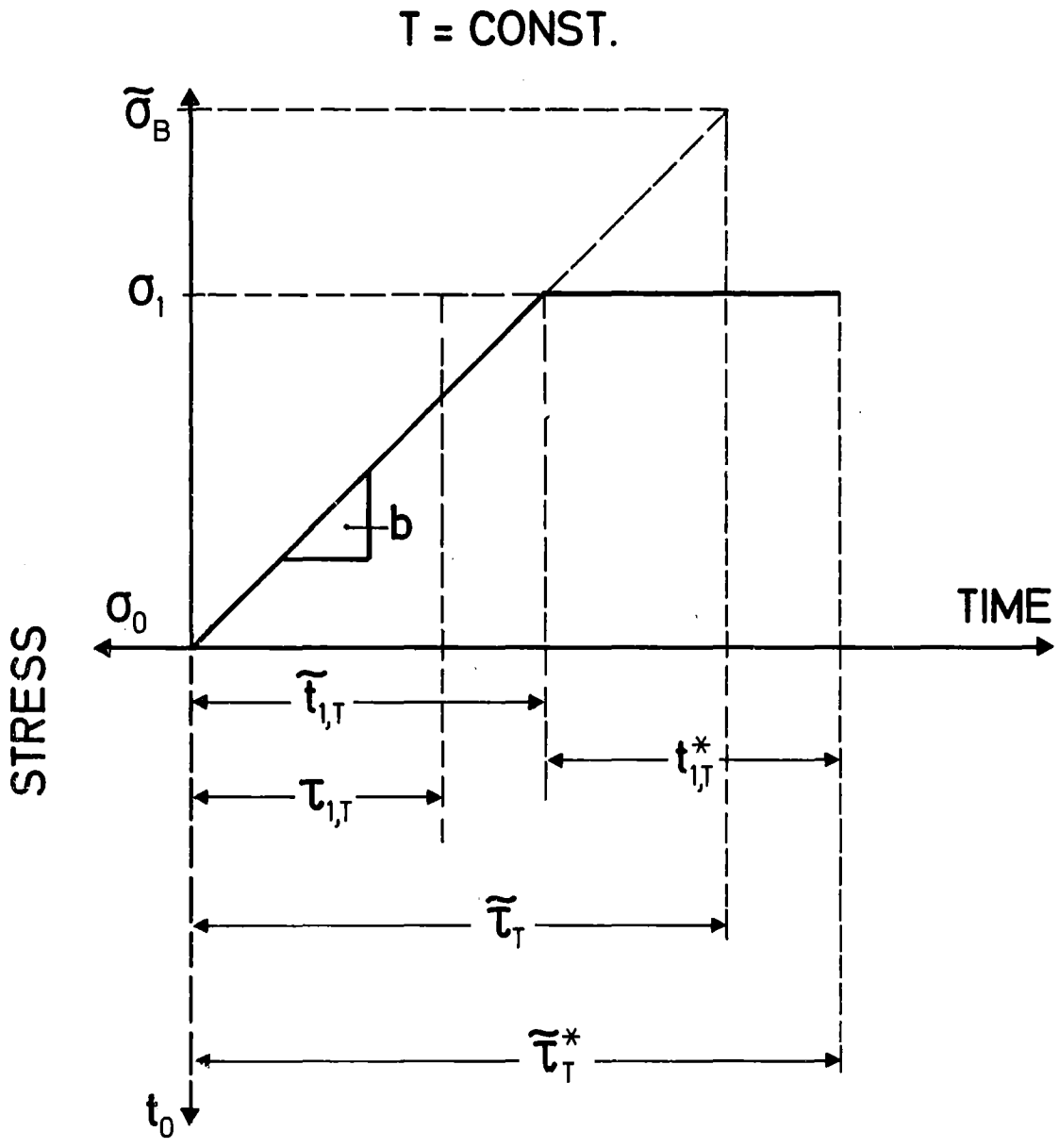

Fig.11 The σ-ramp-hold procedure.

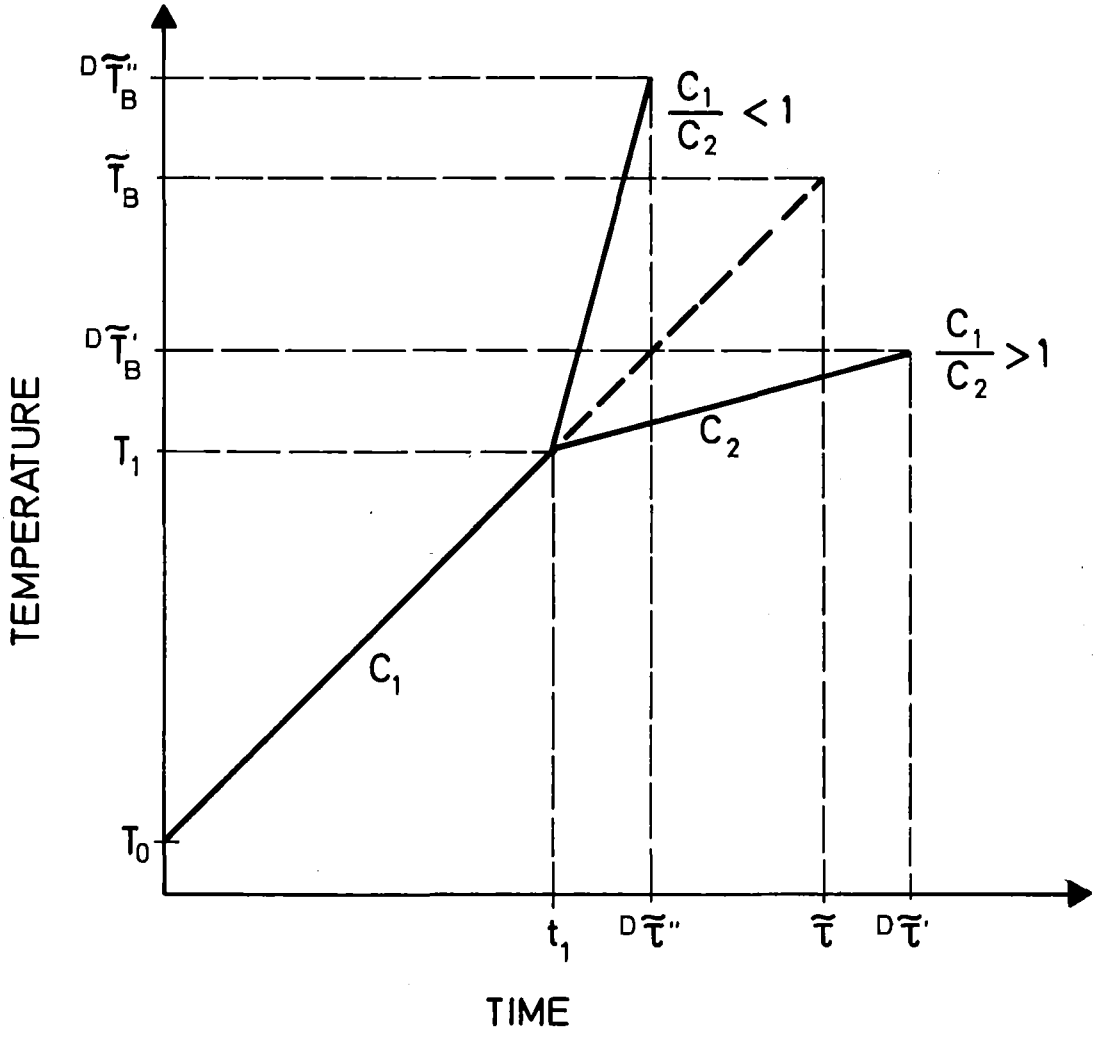

Fig.12 The double T-ramp.

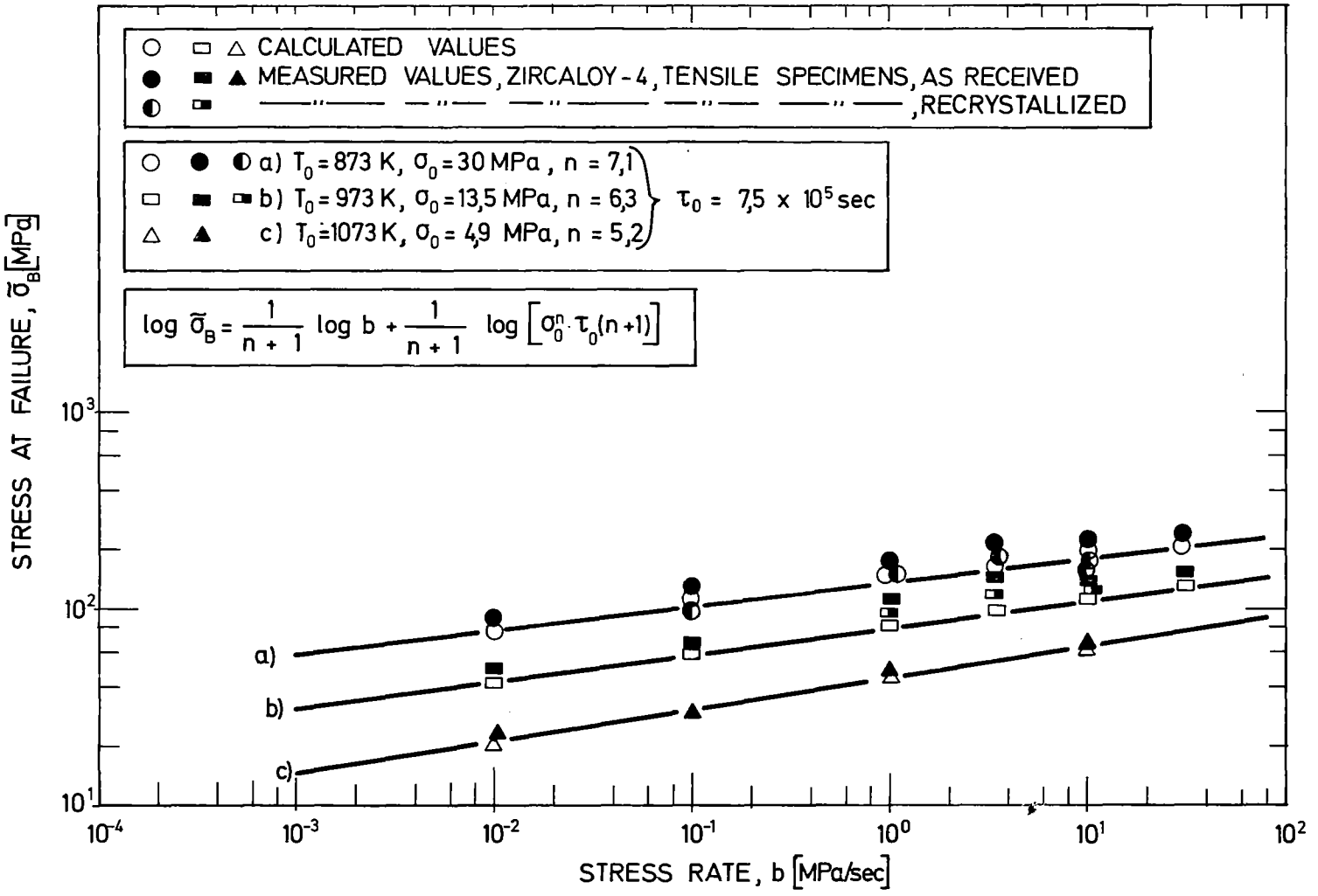

Fig.13 The σ-ramp. The stress at failure vers. stress rate (calculations are represented by solid lines).

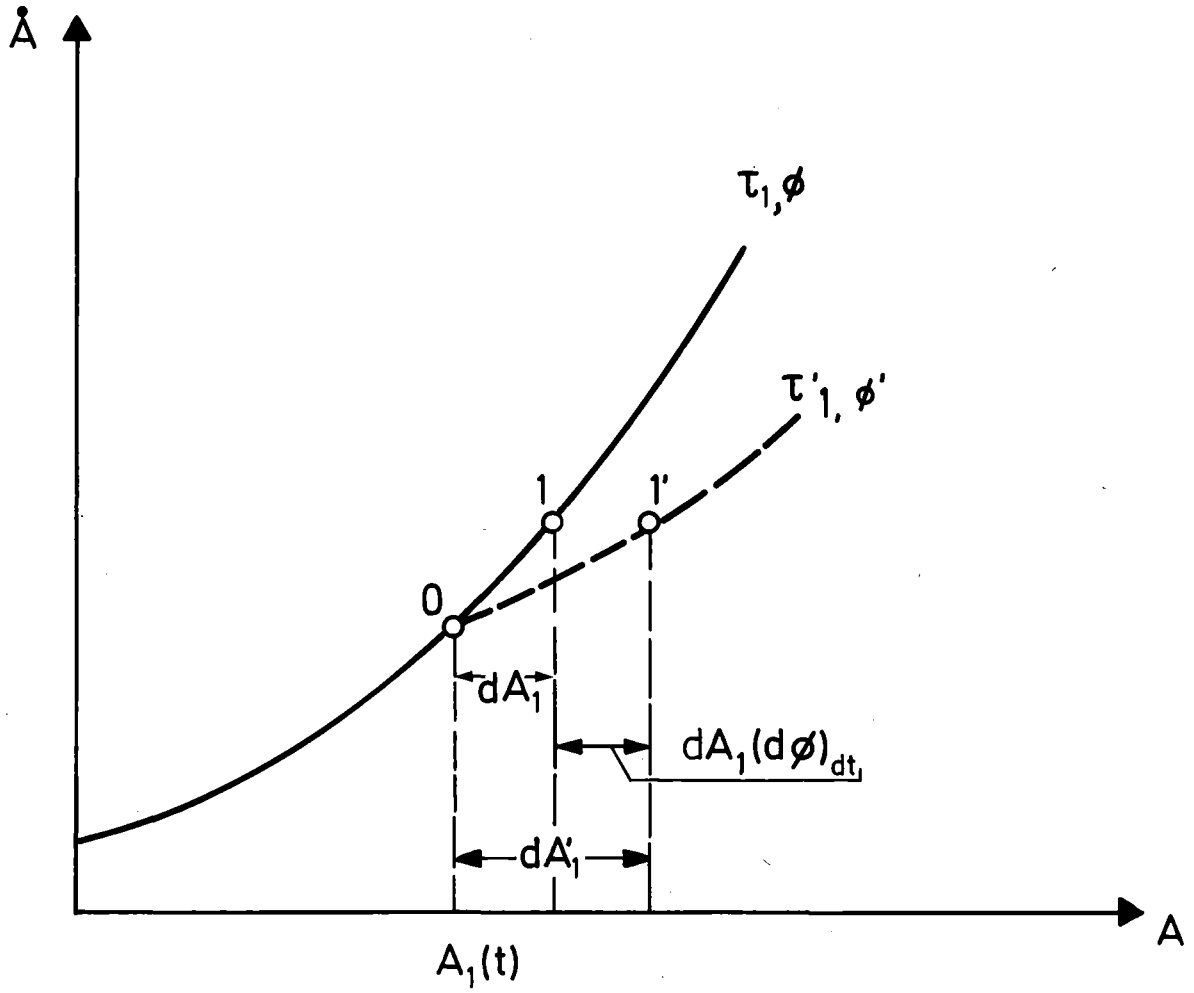

Fig.14 The damage function (see text).

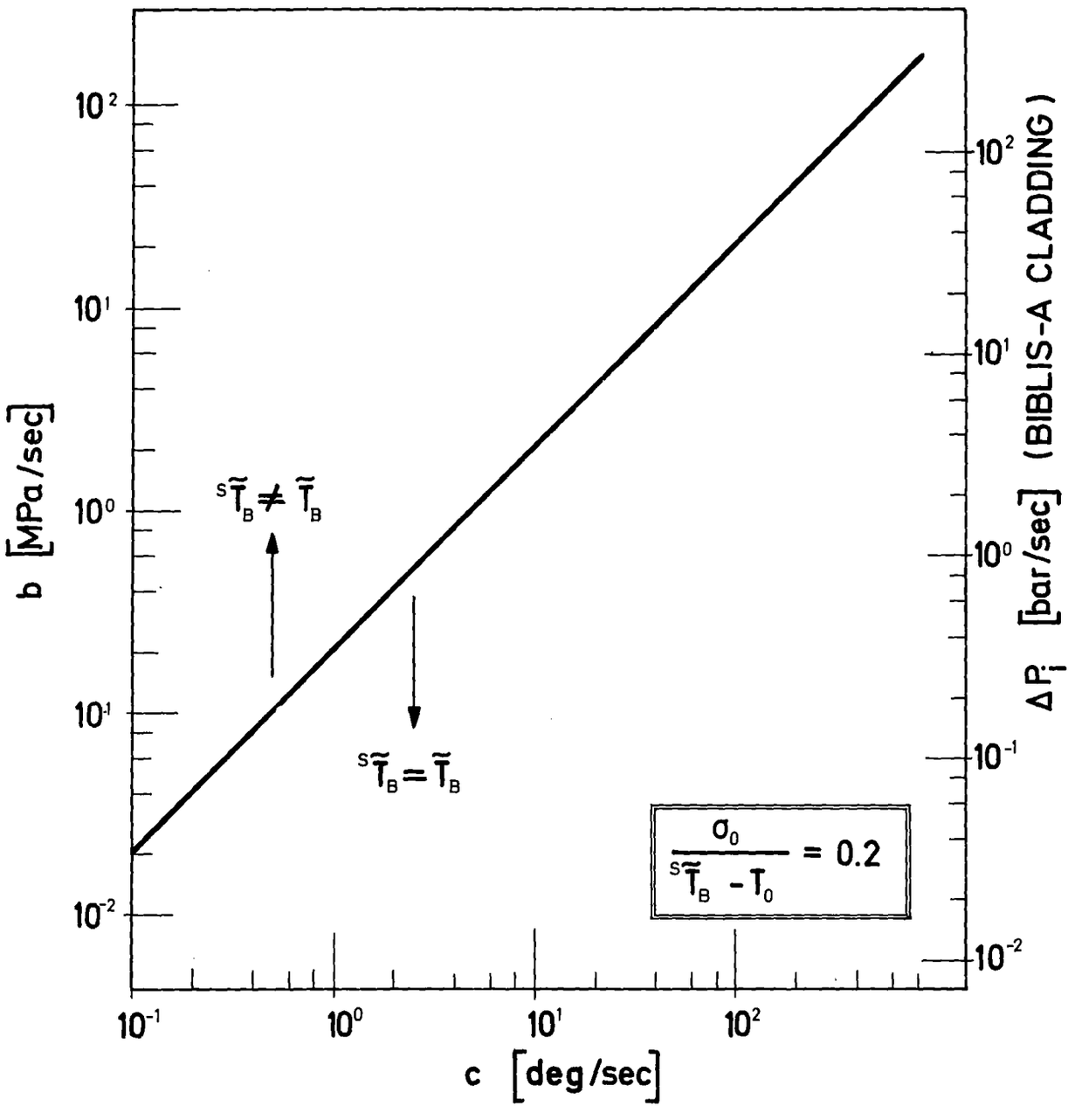

Fig.15 Superimposed ramps (graphical representation of the criterion given by Eq(2.2.4)).

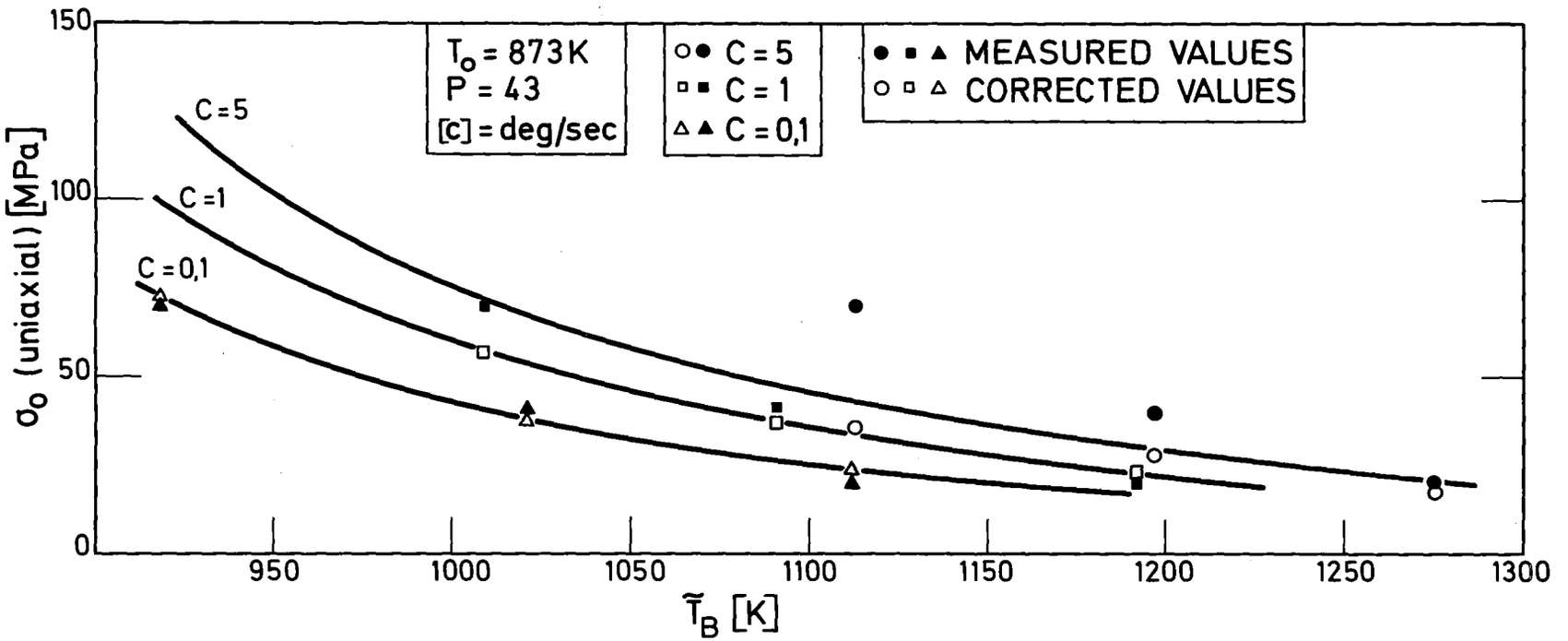

Fig.16 The T-ramp. The temperature at failure vers. stress. Correction of experimental values for temperature differences (calculation represented by solid lines).

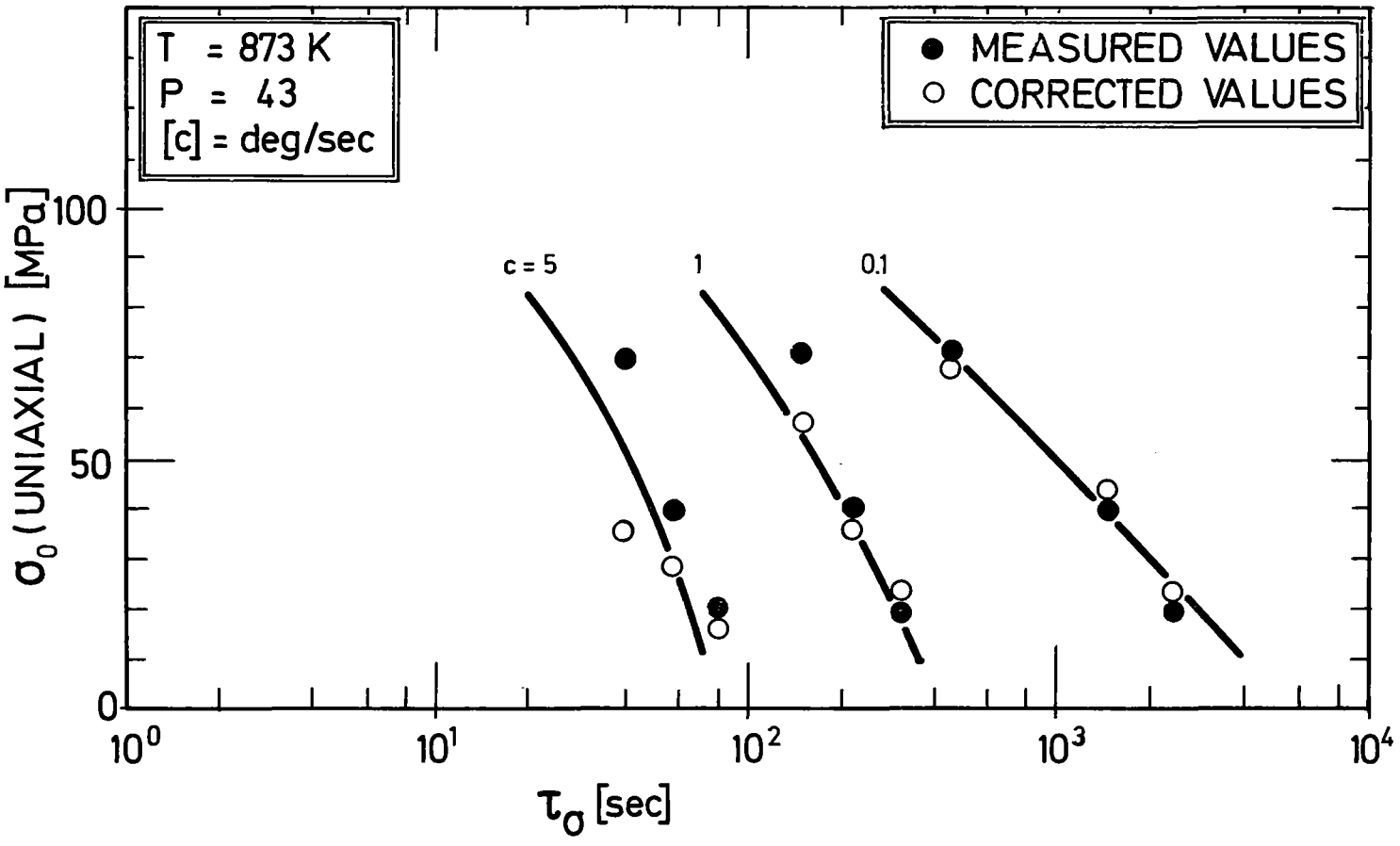

Fig.17 The T-ramp. The life time vers. stress. Correction of experimental values for temperature differences (calculations represented by solid lines).